On the use of path-dependent maximum range method in critical plane based multi-axial fatigue criteria

MSc Thesis

Xinhai Wang

January 25, 2016

Supervisor: Mirek Kaminski

Delft University of Technology

Department of Offshore and Dredging Engineering

Specialization: Structural design and analysis

Abstract

Multi-axial stress state is the stress state where several stress components exist. Multi-axial fatigue assessment is very challenging due to complex stress state and component geometry. Many multi-axial fatigue assessment criteria simplify the complex multi-axial stress into an equivalent uniaxial stress. Critical plane method which bases on observation of fatigue cracking initiation and propagation behavior of smooth specimens is widely used. The critical plane is usually determined by maximizing the amplitudes and/or values of some stress components, and the parameters obtained on the critical plane are used to analyze fatigue strength.

For uniaxial loading, rainflow counting method can be used to evaluate the complex variable-amplitude stress history. However, this method cannot be applied to non-proportional multi-axial stress state. The so-called Path-Dependent Maximum range (PDMR) method is proposed by Zhigang Wei and Pingsha Dong to evaluate complex multi-axial stress history. This method uses the calculated effective stress range at mapped normal-shear stress space to evaluate the fatigue damage.

The aim of this thesis is to explore the feasibility by applying PDMR method to determine equivalent stress amplitude for critical plane method. PDMR matlab algorithm is programed based on publications in literature. Several experimental results related to high cycle fatigue strength for smooth specimens, subjected to proportional or non-proportional loading with different mean stress values and various stress ratios, are analyzed by employing the proposed PDMR based critical plane method and other criteria available in the literature, such as Findley, McDiarmid, Matake, Dang Van, Papadopoulos and modified Carpinteri-Spagnoli (C-S) criterion. The proposed method shows a good estimation capacity as compared to the aforementioned criteria. Also, the proposed critical plane method is extended to estimate the fatigue life for tubular tube-to-plane welded joints under proportional or non-proportional loading.

Fracture plane orientation determination method is proposed based on observation of plotted equivalent stress amplitude on each material plane calculated by PDMR method. This method shows good estimation capacity for the experimental data examined.

Nomenclature

m	Reverse slope value of *S-N* curve	
C_a	Shear stress amplitude	[MPa]
$C_{a,eq}$	equivalent fully reversed shear stress amplitude	[MPa]
$t_1, t_2, \cdots, t_k, \cdots t_N$	Time instants	[sec]
R	Stress ratio	
T	Length of stress history	[sec]
W	Weight function	

Vectors and matrixes

$\mathbf{I_1}$	first stress invariant matrix
I	identity tensor
$\boldsymbol{S_w}$	stress vector on the material plane
C	shear stress vector acting on the material plane
N	normal stress vector perpendicular to the critical plane
u	unit vector on the material plane
v	unit vector on the material plane
w	unit vector normal to the material plane
σ	cartesian stress tensor
$\mathbf{B_i}$	*i*-th components of an orthonormal basis of dev^3
$\mathbf{b}_i$	*i*-th component of an orthonormal basis of $\Re^5$
X	deviatoric stress tensor at material point *P* in dev^3
x	deviatoric stress vector at material point *P* in $\Re^5$

Greek Symbols

α	phase angle between longitudinal normal stress σ_x and tangential normal stress σ_y	[rad]
β	phase angle between longitudinal normal stress σ_x and shear stress τ_{xy}	[rad]
γ	angle between longitudinal axis of the specimen and normal vector **w** to the critical plane	[degree]

η	angle between longitudinal axis of the specimen and normal vector to fatigue fracture plane	[degree]
δ	off angle	[rad]
λ_{xy}	Ratio between frequency ω_{xy}/ω_x	
λ_y	Ratio between frequency ω_y/ω_x	
σ	normal stress	[MPa]
σ_h	hydrostatic stress	[MPa]
σ_1	maximum Principal stress	[MPa]
$\sigma_{af,0}$	fatigue limit for purely pulsating normal stress	[MPa]
σ_{af}	fatigue limit for fully reversed normal stress	[MPa]
σ_f'	fatigue strength coefficient	[MPa]
σ_u	ultimate tensile strength	[MPa]
τ	shear stress	[MPa]
τ_{af}	fatigue limit for fully reversed shear stress	[MPa]
$\hat{\phi}, \hat{\theta}, \hat{\psi}$	expected values of the Euler angles	[rad]
φ, ϑ	angles defining Puvw coordinate system with respect to PXYZ coordinate system	[rad]
ϕ, θ, ψ	Euler angles	[rad]
ω_x	angular frequency of the sinusoidal longitudinal normal stress σ_x	[rad/sec]
ω_y	angular frequency of the sinusoidal tangential normal stress σ_y	[rad/sec]
ω_{xy}	angular frequency of the sinusoidal shear stress τ_{xy}	[rad/sec]

Subscripts

a	amplitude of the stress components
max	maximum value of a given stress component
min	maximum value of a given stress component
m	mean value of a given stress component
A,B	indication of case A or case B crack growth
ij	Element of a given stress component in Cartesian stress tensor

Contents

Acknowledgments

I would like to thank Professor Mirek Kaminski for providing this master thesis topic and his valuable comments and advice.

Also, I would like to thank Paula van Lieshout for her comments of the thesis.

Furthermore, I would like to thank academic counsellor Evert Vixseboxse and psychologist Inge Verhoeven for their help during the process of writing this thesis.

I also would like to thank my parents for supporting my master study abroad at TU Delft.

1. Introduction

Fatigue strength evaluation of the structure components is a major part for designing offshore structures. For simple uniaxial loading, S-N curve can be applied to access the fatigue strength easily. For variable-amplitude uniaxial loading, rainflow counting method can tackle the problem by transforming the complex stress history into so called equivalent stress amplitude. Because of the complex stress states, there are no universal accepted successful method for structure multi-axial fatigue strength assessment (Socie & Marquis, 2000).

Early, static stress parameters are used to evaluate complex multiaxial loading (Niemi, 1995). However, the calculated fatigue strength results tends to be non-conservative under out-of-phase loading conditions (Chen, Gao, & Sun, 1994). Lately, stress invariant and hydrostatic stress are used as fatigue strength parameter to evaluate the multi-axial fatigue strength. For example, Crossland (Crossland, 1956)and Sines (Sines, Waisman, & Dolan, 1959) methods use hydrostatic stress and stress invariant to represent the normal stress component and the shear stress component respectively. And the maximum combination of these two parameters is used to calculate the multi-axial fatigue strength.

Critical plane method such as Papadopoulos (Papadopoulos I. , 1998) and Carpinteri-Spagnoli (Carpinteri & Spagnoli, 2001)is widely used for multi-axial fatigue strength calculation. This method is proposed according to crack initiation and propagation procedure of smooth specimens. After the critical plane is determined, the parameters obtained on the plane is applied to calculate fatigue strength.

Loading path effect is a vital factor need to be considered for multi-axial fatigue strength assessment. Sonsino and Kueppers (Sonsino & Kueppers, 2001) proposed that the out-of-phase loading is more damaging than in-phase loading for ductile materials.

Various counting method such as MCC (Zouain, Mamiya, & Comes, 2006) and PH (Mamiya, Araújo, & Castro, 2009)have been proposed to take non-proportional loading effect into account. Zhigang Wei and Pingsha Dong (Dong, Wei, & Hong, 2010) proposed a path-dependent multi-axial counting method searching effective stress ranges in the mapped normal and shear stress space. This method can not only be used in the 2D normal-shear stress plane, but also in the 3D stress space, such as normal, in-phase shear and transverse shear stresses space. After every stress paths is counted, the equivalent uniaxial stress amplitude can be calculated by applying Miner's rule.

According to the experiment conducted by Smith, Sines states that mean shear stress is negligible for components under cyclic shear stress loading (Kluger, 2015). In the HCF range, many multiaxial fatigue criterion only consider the mean normal stress effect.

This master thesis aims to explore the feasibility of applying PDMR based method to define the critical plane and corresponding equivalent uniaxial stress. First, the background knowledge for multi-axial fatigue evaluation is introduced. Then, various multi-axial fatigue criterions form literature are presented and compared. Last, the proposed PDMR based critical plane method and other critical plane methods from literature are applied to access experimental results from published literature. After comparison of results, the effectiveness and accuracy of proposed PDMR 3D critical plane method could be acquired.

2. Literature Review

2.1. Stress Analysis

2.1.1. Static Stress Analysis

For the case of 3D-stress state, the stresses at a generic point P can be represented by stress tensor **σ** as follows:

$$\boldsymbol{\sigma} = \begin{bmatrix} \sigma_x & \tau_{xy} & \tau_{xz} \\ \tau_{yx} & \sigma_y & \tau_{yz} \\ \tau_{zx} & \tau_{zy} & \sigma_z \end{bmatrix} \tag{2.1}$$

Tensile stress is defined as positive while compressive stress is defined as negative. When tensile stress is acting on the plane, positive shear stress direction on the plane is define as positive direction of the coordinate axes. Positive directions of normal and shear stresses at a generic point are shown in Figure 2.1.a.

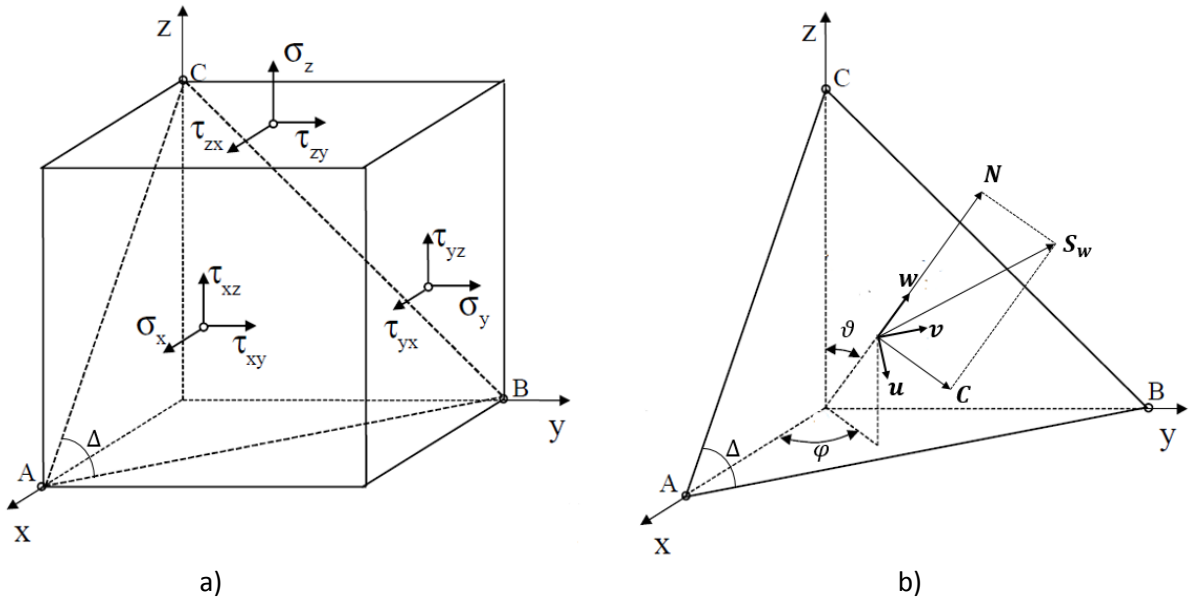

a) b)

Figure 2.1. a) Stress components of a stress tensor at a generic point and b) stress tensor on the material plane Δ.

Considering two orthogonal unit vectors, **u** and **v**, on the material plane **Δ**. Vector **u** is defined as on the ***wZ***-plane. Note that **Z**-axis perpendiculars both the ***XY***-plane and the vector **v**, so the vector **v** is on the ***XY***-plane (Figure 2.2). The direction cosine of the vector **w** is determined with respect to P_{XYZ} by using φ and ϑ in the spherical coordinate system.

$$\boldsymbol{w}^{\mathrm{T}} = [sin\vartheta\cos\varphi \quad \sin\vartheta\sin\varphi \quad \cos\vartheta] \tag{2.2}$$

The direction cosines of **u** and **v** can also be calculated with respect to P_{XYZ}.

$$\boldsymbol{u}^{\mathrm{T}} = [cos\vartheta\cos\varphi \quad \cos\vartheta\sin\varphi \quad -\sin\vartheta] \tag{2.3}$$

$$\boldsymbol{v}^{\mathrm{T}} = [-sin\varphi \quad \cos\varphi \quad 0] \tag{2.4}$$

The stress vector $\boldsymbol{S}_w$ on Δ is given by

$$\boldsymbol{S}_w = \boldsymbol{\sigma w} \tag{2.5}$$

The stress vector $\boldsymbol{S}_w$ is composed of normal stress vector **N** and shear stress vector **C** as

$$N = (\boldsymbol{\sigma w} \cdot \boldsymbol{w}) \quad \boldsymbol{N} = N\boldsymbol{w} \tag{2.6}$$

and

$$\boldsymbol{C} = \boldsymbol{S}_w - \boldsymbol{N} \tag{2.7}$$

where the dot in Eq.(2.6) is scalar product. Shear stress $\boldsymbol{C}$ magnitude can be computed by Eq. (2.8) as follows

$$C^2 = \boldsymbol{C}^T\boldsymbol{C} = \boldsymbol{S}_w^T\boldsymbol{S}_w - N^2 \tag{2.8}$$

Shear stress vector $\boldsymbol{C}$ on the plane Δ can be decomposed into **u** and **v** direction.

$$\boldsymbol{C}_u = (\boldsymbol{C} \cdot \boldsymbol{u})\boldsymbol{u} \quad \boldsymbol{C}_v = (\boldsymbol{C} \cdot \boldsymbol{v})\boldsymbol{v} \tag{2.9}$$

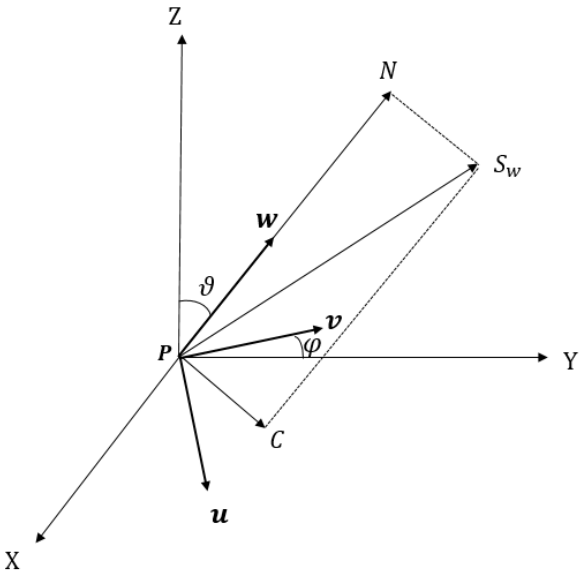

Fig. 2.2. P_{uvw} and P_{XYZ} coordinate systems

2.1.2. Principal stresses and stress invariants

The principal stresses are the stresses of stress tensor when only normal stress components exist. The principal stresses and corresponding directions are the eigenvalues and corresponding eigenvectors of the stress tensor. The eigenvalues and corresponding eigenvectors can be calculated by solving the following equations:

$$\left(\sigma_{ij} - \sigma\delta_{ij}\right)n_j = 0 \tag{2.10}$$

Where σ_{ij} is the stress tensor, σ is eigenvalue, δ_{ij} is the Kronecker delta and $n_j$are corresponding eigenvectors. The determinant need to be zero to get non-trivial eigenvectors:

$$\left|\sigma_{ij} - \sigma\delta_{ij}\right| = \begin{vmatrix} \sigma_x - \sigma & \tau_{xy} & \tau_{xz} \\ \tau_{yx} & \sigma_y - \sigma & \tau_{yz} \\ \tau_{zx} & \tau_{zy} & \sigma_z - \sigma \end{vmatrix} = 0 \tag{2.11}$$

The following characteristic equation can be get:

$$\sigma^3 - I_2\sigma^2 + I_2\sigma - I_3 = 0 \tag{2.12}$$

With

$$I_1 = \sigma_x + \sigma_y + \sigma_z \tag{2.13}$$

$$I_2 = \sigma_x\sigma_y + \sigma_y\sigma_z + \sigma_x\sigma_z - \tau_{xy}^2 - \tau_{yz}^2 - \tau_{xz}^2 \tag{2.14}$$

$$I_3 = \sigma_x\sigma_y\sigma_z + 2\tau_{xy}\tau_{yz}\tau_{zx} - \tau_{xy}^2\sigma_z - \tau_{yz}^2\sigma_x - \tau_{zx}^2\sigma_y \tag{2.15}$$

Where I_1, I_2 and I_3 is first, second and third stress invariants, respectively. These stress invariants are constant.σ_1,σ_2 and σ_3 is the first, second and third principal stress, respectively. Eigenvectors describe the direction of corresponding principal stresses.

2.1.3. Deviatoric stress and invariants

Considering a stress tensor σ_{ij} acting at a generic point. Stress tensor σ_{ij} can be divided into hydrostatic stress and deviatoric stress. Deviatoric stress tensor can be calculated as follows:

$$s_{ij} = \sigma_{ij} - \boldsymbol{\sigma}_h \tag{2.16}$$

The hydrostatic stress tensor is defined as:

$$\boldsymbol{\sigma}_h = \sigma_h \boldsymbol{I} = \frac{1}{3}(\sigma_x + \sigma_y + \sigma_z)\boldsymbol{I} \tag{2.17}$$

After getting the deviatoric stress tensor, the first, second and third deviatoric stress invariants and corresponding directions can be calculated with the similar procedure for principal stress described in 2.1.2. J_1, J_2 and J_3 can be expressed as follows:

$$\begin{gathered} J_1 = 0 \\ J_2 = \frac{1}{2}s_{ij}s_{ji} = \frac{1}{6}\left[(\sigma_x - \sigma_y)^2 + (\sigma_y - \sigma_z)^2 + (\sigma_z - \sigma_x)^2\right] + \tau_{xy}^2 + \tau_{yz}^2 + \tau_{zx}^2 \\ J_3 = det(s_{ij}) = \frac{1}{3}s_{ij}s_{jk}s_{ki} \end{gathered} \tag{2.18}$$

2.1.4. Mean stress effect

Based on the experiment conducted by Smith, Sines (Sines, Waisman, & Dolan, 1959) states mean shear stress is negligible for structure components under sinusoidal shear stress loading In the HCF range. In this thesis, only the mean normal stress effect is considering for the multi-axial fatigue strength calculation.

Gerber (Gerber, 1874)use ultimate strength as a correction factor and get the following equation:

$$\sigma_{eq,a} = \sigma_a / \left(1 - (\frac{\sigma_m}{\sigma_u})^2\right) \tag{2.19}$$

$\sigma_{eq,a}$ is equivalent fully reversed stress amplitude, σ_a is stress amplitude and σ_m is mean stress value, σ_u is ultimate strength value.

The main drawback of the Gerber method is that it cannot distinguish between compression and tension. It is apparent that tension is detrimental to the fatigue strength while the compression is on the contrary.

Goodman's (Goodman, 1899) method is very similar to Gerber's and the compression and tension effect is distinguished:

$$\begin{aligned} \sigma_{eq,a} &= \frac{\sigma_a}{\left(1-\frac{\sigma_m}{\sigma_u}\right)} \qquad for\ \sigma_m > 0 \\ \sigma_{eq,a} &= \sigma_a \qquad for\ \sigma_m \ll 0 \end{aligned} \tag{2.20}$$

Susmela (Susmela, Tovoa, & Lazzarin, 2005) uses yield strength of the material as a correction factor and get the following equation:

$$\begin{aligned} \sigma_{eq.a} &= \frac{\sigma_a}{\left(1-\frac{\sigma_m}{\sigma_y}\right)} \qquad for\ \sigma_m > 0 \\ \sigma_{eq.a} &= \sigma_a \qquad for\ \sigma_m \ll 0 \end{aligned} \tag{2.21}$$

Dowling (Dowling, 2009) use fatigue strength coefficient of the material as a correction factor and get the following equation:

$$\begin{aligned} \sigma_{eq.a} &= \frac{S_a}{\left(1-\frac{S_m}{\sigma_f'}\right)} \qquad for\ \sigma_m > 0 \\ \sigma_{eq.a} &= \sigma_a \qquad for\ \sigma_m \ll 0 \end{aligned} \tag{2.22}$$

The Smith-Watson-Topper (Susmela, Tovoa, & Lazzarin, 2005) method bases on Mode I growth and can be expressed as follows:

$$\sigma_{ar} = \sqrt{\sigma_{max}\sigma_a} = \sigma_a\sqrt{\frac{2}{1-R}} = \sigma_{max}\sqrt{\frac{1-R}{2}} \tag{2.23}$$

2.1.5. Dynamic stress analysis

For in-phase loading, the stress components histories can be expressed by following equation:

$$\sigma_{ij}(t) = \sigma_{ij,m} + \sigma_{ij,a}\sin(\omega t) \tag{2.24}$$

Where $\sigma_{ij,m}$ is stress mean value, $\sigma_{ij,a}$ is stress amplitude. ω is stress frequency.

For non-proportional loading, the stress components history can be expressed as follows:

$$\sigma_{ij}(t) = \sigma_{ij,m} + \sigma_{ij,a}\sin(\lambda_{ij}\omega_{ij}t - \alpha_{ij}) \tag{2.25}$$

Where λ_{ij} is the frequency ratio and α_{ij} is the phase angle.

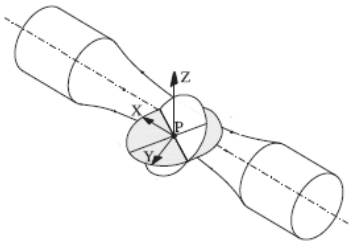

Fig. 2.3. Cylindrical specimen

The stress histories at the generic point *P* of a specimen (Fig.2.3.) under sinusoidal normal and shear stress loading can be expressed by following equations:

$$\begin{aligned} \sigma_x &= \sigma_{x,m} + \sigma_{x,a}\sin(\omega_x t) \\ \sigma_y &= \sigma_{y,m} + \sigma_{y,a}\sin(\omega_y t - \alpha) \\ \tau_{xy} &= \tau_m + \tau_a \sin(\omega_{xy} t - \beta) \end{aligned} \tag{2.26}$$

As shown in 2.4., the stress vector history $\boldsymbol{S}_w(t)$ on the material plane Δ can be divided into normal stress vector history $\boldsymbol{N}(t)$ and shear stress vector history ***C***(t) (B. Li & Freitas, 2009).

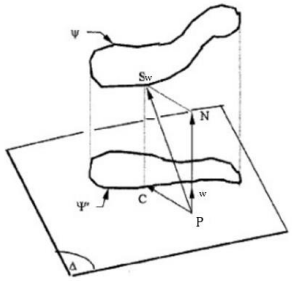

Fig. 2.4. Stress S_w on the material plane Δ

Since the direction of normal stress vector $\boldsymbol{N}$ is normal to the material plane Δ, amplitude of the normal stress $\boldsymbol{N_a}$ and mean value of normal stress $\boldsymbol{N_m}$ is easy to calculate. Because direction of shear stress vector history Ψ' is changing with time, calculation of shear stress amplitude is quite complicated. Various methods has been proposed to define shear stress amplitude, such as: Longest Projection method (V & A., 1976), the Longest Chord method (Lemaitre & Chaboche, 1990), the Minimum Circumscribed Circle (MCC) method (Zouain, Mamiya, & Comes, 2006) (Li, Reis, & Freitas, 2009) and the Prismatic Hull (PH) method (Mamiya & Araújo, 2002) (Mamiya, Araújo, & Castro, 2009) (Gonçalves, Araújo, & Mamiya, 2005) (Araújo, Dantas, Castro, Mamiya, & Ferreira, 2011).

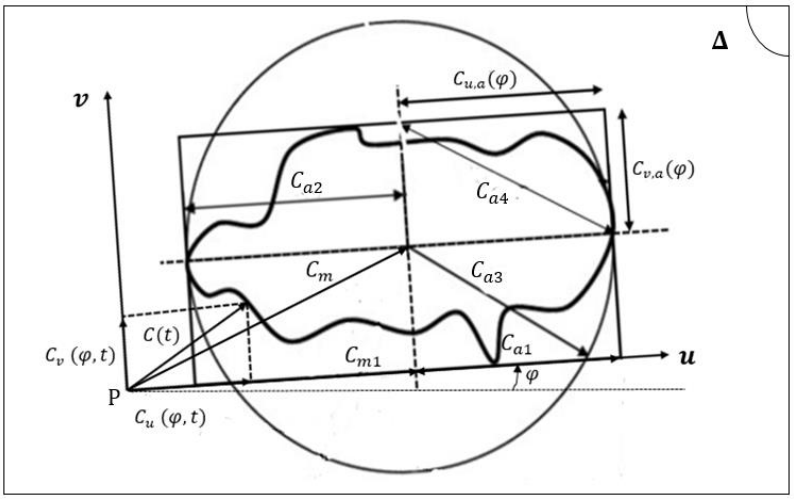

Fig. 2.5. Amplitude and mean value (C_{a1}, C_{m1}), (C_{a2}, C_m), (C_{a3}, C_m) and (C_{a4}, C_m) of stress history Ψ' on the material plane calculated by the LP, LC, MCC and PH methods.

Mean and amplitude of stress history determined by aforementioned various method for a complex loading history is shown in Fig. 2.5. The longest projection method searches for the maximum projection of stress history Ψ' to a line tangent to the stress history. The amplitude of stress history is defined as half-length of projection. Mean value is defined as the middle point of projection line. Longest chord method searches longest chord in the stress history Ψ'. Stress amplitude is defined as half-length of the longest chord. Mean stress is defined as the longest chord middle point. Minimum circumscribed circle method searches the minimum circle that encloses stress history Ψ'. Stress amplitude is defined as radius of the enclosed minimum circle. Mean stress is defined as the center of enclosed circle.

Longest projection, longest cord and minimum circumscribed circle method cannot differentiate out-of-phase and in-phase stress histories. For example, a linear stress history and a circle stress history with diameter equal to the linear stress length will be defined having the same stress amplitude and mean value according to those methods.

Araújo et al. (Araújo, Dantas, Castro, Mamiya, & Ferreira, 2011) proposes the maximum rectangular hull method to define shear stress amplitude on material planes. This method searches the maximum rectangular hull which is tangent to the shear history on the material planes. Considering a specific shear stress history Ψ' on the material plane Δ(Fig.2.5), the orthonormal vectors **u** and **v,** which can be defined with respect to direction of x axis in this thesis, can define the half-length of the sides of rectangular hulls as follows:

$$C_{u,a}(\varphi) = \frac{1}{2}\left[\max_{0\le t<T} C_u(t,\varphi) - \min_{0\le t<T} C_u(t,\varphi)\right] \tag{2.27a}$$

$$C_{v,a}(\varphi) = \frac{1}{2}\left[\max_{0\le t<T} C_v(t,\varphi) - \min_{0\le t<T} C_v(t,\varphi)\right] \tag{2.28b}$$

For each φ-oriented rectangular hull, stress amplitude C_a of stress history Ψ' is define as half-length of diagonal of rectangular hull:

$$C_a = \max_{0\le t<T} \sqrt{\left[C_{u,a}(\varphi)\right]^2 + \left[C_{v,a}(\varphi)\right]^2} \tag{2.29}$$

It is obvious that only the points of shear stress history Ψ' that belonging to the largest rectangular hull is used to define the stress amplitude according to the MCH method, which may be a drawback compared to PDMR method which uses every point of the stress history Ψ'.

2.2. Fracture procedure

There are three basic fracture modes shown in Figure 2.6. Mode I corresponds to tension, mode II corresponds to in-plane shear and mode III corresponds to out-of-plane shear.

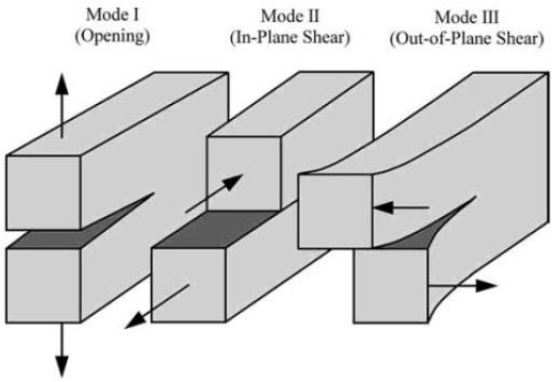

Figure 2.6. Fracture mode (Anderson, 2005)

Crack development until final fracture can be divided into three stages: crack initiation stage, crack propagation stage and final fracture stage. Different mechanism control these stages. At the first stage, crack nucleation occurs along shear slip band. Many critical plane methods define the shear ship plane as the critical plane (Carpinteri, Spagnoli, & Vantadori, 2009). The critical plane is the plane on which the stresses are used to do the fatigue evaluation. At the second stage, crack propagates along the plane which is normal to the direction of maximum principal stress (Carpinteri, Spagnoli, & Vantadori, 2009). This plane is the fracture plane observed from the experiments. And the orientation of the two planes at stage one and stage two is different (Carpinteri, Spagnoli, & Vantadori, 2009).

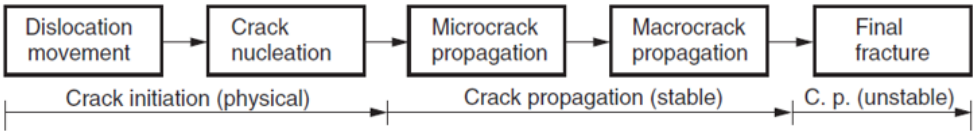

Figure 2.7. Crack develop procedure (Radaj, Sonsino, & Fricke, 2006)

Crack propagate plane is assumed normal to the direction of maximum principal stress. Crack initiate plane, which is the critical plane defined by critical plane method, can be obtained relate to fracture plane using off angle given as follows (Carpinteri, Brighenti, & Spagnoli, 2000):

$$\delta = \frac{3\pi}{8}[1 - (\frac{\tau_{af}}{\sigma_{af}})^2] \tag{2.30}$$

Off angle δ is the angle between vector **w** and direction of averaged maximum principal stress direction $\hat{1}$, in averaged principal plane $\hat{1}\hat{3}$(Fig.2.8).

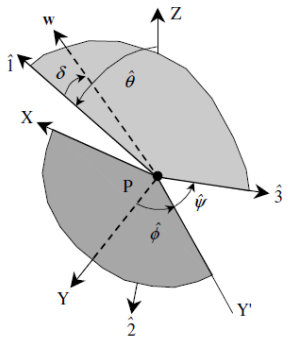

Fig.2.8. off angle δ (Carpinteri, Spagnoli, & Vantadori, 2009)

For hard metal ($\tau_{af}/\sigma_{af} > 1$), δ is assumed to be 0. So the fracture plane coincides with critical plane For mild metal, δ is assumed to be $\pi/4$.

2.3. SN curve

The S-N curve presents the relationship between stress range and number of load cycles to failure on logarithmic scale. Under constant amplitude loading, the relationship can be defined as:

$$N(\Delta S)^m = C \tag{2.31}$$

N is cycles to failure, ΔS is stress range, C and m are material dependent constant.

Fatigue limit is defined in S-N curves. Fatigue failure will occurs when stress range is bigger than fatigue limit.

2.4. Multi-axial cycle counting

For simple cyclic constant amplitude uniaxial loading, it is very easy to define the amplitude and corresponding cycle. However, for complex asynchronous variable amplitude stress histories, it is very difficult to define equivalent stress amplitude and corresponding cycles. There are many methods proposed by different authors to transform the random stresses history into equivalent uniaxial stresses.

2.3.1.1. Bannantine & Socie

Bannantine & Socie (Bannantine & Socie, 1992) states that according to the different loading type, different crack modes (as stated in 2.2) develop. Damage caused by normal and shear stress needed to be calculated according to uniaxial rainflow counting respectively, and the large damage value will be used for fatigue evaluation (Bannantine & Socie, 1992). Because the calculation is processed separately, so the out-of-phase effect is not taken into account (Dong, Wei, & Hong, 2010).

2.3.1.2. Wang & Brown

Early, the static stress parameter such as von Mises stress is used for multi-axial fatigue calculation (Niemi, 1995), since the von Mises stress value is always positive, which will lead mistake for 90 out-of-phase loading (Meggiolaro & Castro, 2012).

Wang and Brown (Wang & Brown, 1996) proposed a relative effective von Mises strain parameter to solve this problem.

$$\varepsilon_{RMises} = \frac{\sqrt{\left(\Delta\varepsilon_x - \Delta\varepsilon_y\right)^2 + (\Delta\varepsilon_x - \Delta\varepsilon_z)^2 + \left(\Delta\varepsilon_y - \Delta\varepsilon_z\right)^2 + 1.5\left(\Delta\gamma_{xy}^2 + \Delta r_{xz}^2 + \Delta r_{yz}^2\right)}}{\sqrt{2}\cdot(1+\bar{\nu})} \quad (2.32)$$

Where $\bar{\nu}$ is effective Poisson coefficient, which is calculated according to the ratio of plastic and elastic strain. $\Delta\varepsilon_x \equiv \varepsilon_{xj} - \varepsilon_{xi}, \Delta\varepsilon_y \equiv \varepsilon_{yj} - \varepsilon_{yi}, \Delta\varepsilon_z \equiv \varepsilon_{zj} - \varepsilon_{zi}, \Delta\gamma_{xy} \equiv \gamma_{xyj} - \varepsilon_{xyi}, \Delta\gamma_{xz} \equiv \gamma_{xzj} - \varepsilon_{xzi}, \Delta\gamma_{yz} \equiv \gamma_{yzj} - \varepsilon_{yzi}$, and $j > i$.

Wang & Brown's multiaxial counting method is quoted below (Meggiolaro & Castro, 2012):

1. The fist counting point should always be the point corresponding to maximum Mises strain.

2. With the initial maximum Mises strain point, the next peek or valley point is searched.

3. When the maximum relative Mises strain or previous path is searched, the final point is acquired.

A complex multiaxial load path in Fig.2.9 is taken from (Meggiolaro & Castro, 2012) for the purpose of illustration. The point A corresponding to the maximum absolute Mises strain is the first point. The relative equivalent strain is calculated using the aforementioned equation. According to Wang & Brown's method, the path $\mathrm{ABB'F}$ give the maximum relative Mises strain. So the next initial counting point is B. The procedure for the first two counting is illustrated in Fig 2.10. and 2.11.

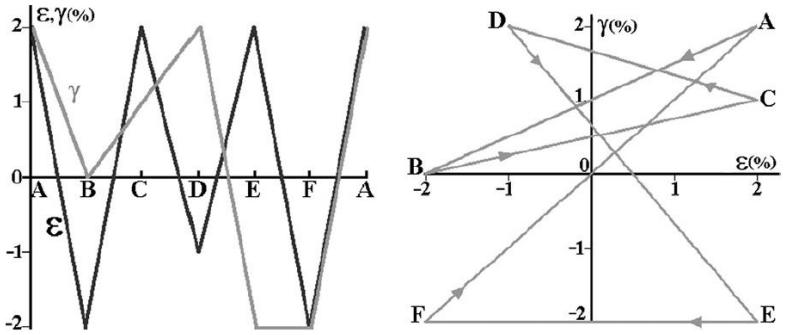

Figure 2.9. Normal and shear strain history (left) and normal-shear strain plot (right) (Meggiolaro & Castro, 2012)

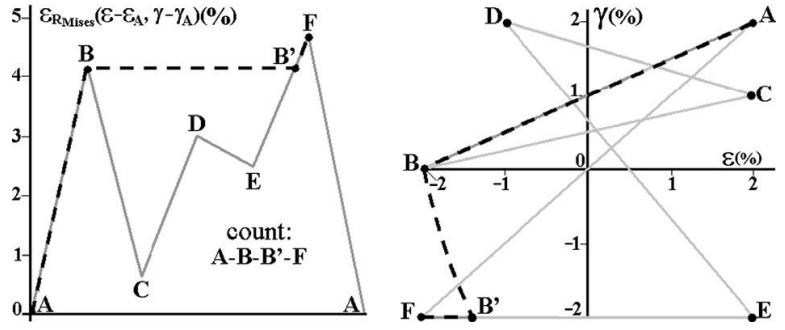

Figure 2.10. First cycle count (Meggiolaro & Castro, 2012)

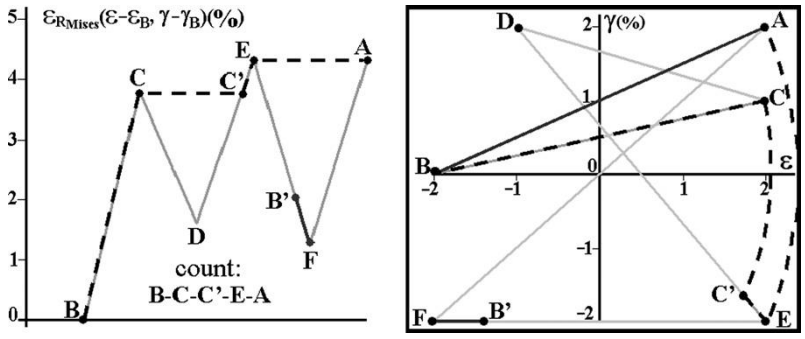

Figure 2.11. Second cycle count (Meggiolaro & Castro, 2012)

2.3.1.3. Path-dependent maximum range

Dong & Hong (Dong, Wei, & Hong, 2010) propose a path-dependent maximum range multi-axial counting method which gets the exact same result as rainflow counting method for uniaxial stress counting. For Wang & Brown method, the point corresponding to the maximum strain value is searched firstly, maximum stress amplitude cannot be counted for some loading cases (Dong, Wei, & Hong, 2010), while for PDMR method, the maximum range of entire stress or strain history is searched firstly. The distance or the so called range is counted as half cycle for this procedure (Dong, Wei, & Hong, 2010).

A simple stress history for the purpose of illustration is shown in Fig.2.12, since the range from P to Q is monotonously increasing, stress range ΔS_e corresponding to the maximum range PQ is defined and half cycle is counted (Dong, Wei, & Hong, 2010).

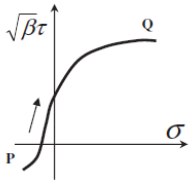

Figure 2.12. Path-dependent maximum range method searching procedure (Dong, Wei, & Hong, 2010).

β is the fatigue strength equivalency factor, which is the ratio between normal stress range and shear stress range in the stress history (Dong, Wei, & Hong, 2010). The parameter is normally between 2 and 4 for steel (Dong, Wei, & Hong, 2010).

Another cycle counting procedure for more complicated stress path is shown in Fig.2.13 (Dong, Wei, & Hong, 2010).

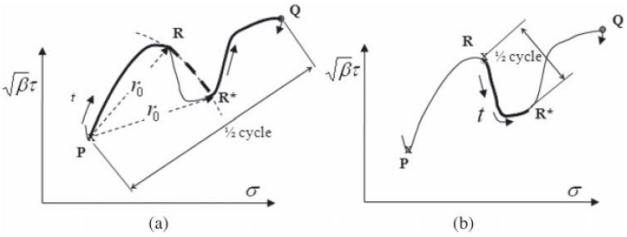

Figure 2.13. PDMR counting procedure in a normal and shear stress space (a) first counted half cycle and (b) second counted half cycle (Dong, Wei, & Hong, 2010)

From point P to R, distance to P is monotonously increasing. From point R to R^*, the distance to P is decreasing, so the first turning point R is get. Distance from R to P and distance from R^* to P is the same, so R^* is the projected turning point. From the point R^* to Q, distance to P is also monotonously increasing. The maximum distance in this loading history is PQ, so the first half cycle is counted. Effective stress range in this cycle is define as real path add virtual path. The real path (solid line in Figure 2.12(a)) is equal to length PR and length R^*R. Virtual path is define as the dashed line in the Figure 2.12(a). Since the distance from the point R to R^* is monotonously increasing. The solid line in the Figure 2.12(b) is the second cycled counted. Effective stress range is length RR^*.

The path length can be expressed as follows:

$$\Delta S_e^{(i)} = \int d\, S_e^i = \int \sqrt{(S_\sigma)^2 + \beta(S_\tau)^2} \tag{2.33}$$

Every point belonging to the normal and shear stress space is used for the counting procedure. Path-dependent maximum range method can be used to analysis asynchronous variable amplitude stress history (Wei & Dong, 2010).

After every half cycle is counted, Mine's rule can be applied to get corresponding equivalent uniaxial stress range as follows (Dong, Wei, & Hong, 2010):

$$\Delta S_{eq} = (\frac{1}{N_R}\sum_i n_i \Delta s_i^m)^{\frac{1}{m}} \tag{2.34}$$

N_R is the total number of cycles counted, m is the exponent of S-N curve. n_i is the number of cycle counted for stress range Δs_i.

The PDMR method can also be applied to three stress space (Dong, Wei, & Hong, 2010). A stress history in 3D space (N(t), C_u(t) and C_v(t)) is shown in Figure 2.15 for the purpose of illustration.

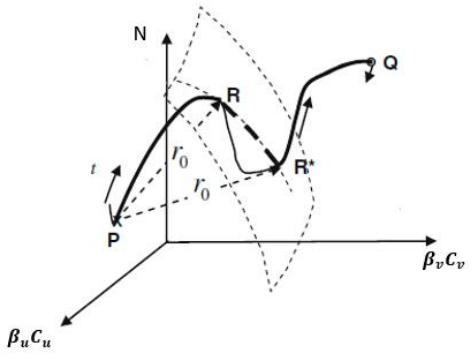

Figure 2.15. PDMR applications 3-D

From the point P to R, the distance to point P is monotonously increasing. From the point P to R^*, distance to point P is decreasing. So the point R is the turning point. Distance from R to P and distance from R^* to P is the same, so R^* is the projected turning point. The path length in 3D space is expressed as follows:

$$\Delta S_e^{(i)} = \int dS_e^i = \int \sqrt{(dN)^2 + \beta_u (dC_u)^2 + \beta_v (dC_v)^2} \tag{2.35}$$

2.5. Multi-axial fatigue criteria

The multi-axial fatigue evaluation criteria could be divided into three main types: stress based criteria, strain based criteria and energy based criteria (Sines, Waisman, & Dolan, 1959). For high cycle multi-axial fatigue calculation, stress-based criteria is usually used (Araújo, Dantas, Castro, Mamiya, & Ferreira, 2011). Most of stress-based criterions transform the multiaxial stress to an equivalent uniaxial stress to calculate fatigue strength with parameters obtained from uniaxial fatigue test (Wang & Yao, 2004). In this thesis, only stress-based multi-axial fatigue criteria is used because it is simplicity and suitability for the engineering practice.

An important procedure for the multi-axial fatigue calculation is to determine the relationship between normal stress damage and shear stress damage (Anes, Reis, Li, Fonte, & Freitas, 2014). The stress-based method could be divided into critical plane criteria, stress invariant criteria, empirical equivalent stress based criteria and integral criteria (You & Lee, 1996).

2.5.1. Empirical equivalent stress

Empirical equivalent stress method use the parameters from static yield theories to combine the normal and shear stress component to calculate the multiaxial fatigue (Li, Jiang, Han, & Li, 2015). However, the predicted results are non-conservative for non-proportional loading condition (Anes, Reis, Li, Fonte, & Freitas, 2014).

2.5.1.1. Von-Mises

The second deviatoric stress can be expressed with only principal stresses as follows:

$$J_2 = \frac{1}{6}\left[(\sigma_x - \sigma_y)^2 + (\sigma_y - \sigma_z)^2 + (\sigma_z - \sigma_x)^2\right] \tag{2.36}$$

For the uniaxial loading condition, where $\sigma_y = \sigma_z = 0$, second deviatoric stress is simplified as follows:

$$\sqrt{J_2} = \frac{\sigma_x}{\sqrt{3}} \tag{2.37}$$

According to von Mises yield criterion, material will yield when second deviatoric stress is larger than yield stress under pure shear loading, the following equation can be acquired:

$$\sqrt{3}\tau_{xy} = \sigma_x \tag{2.38}$$

For 2D stress state, the equivalent stress amplitude can be simplified as follows:

$$\sigma_{eq} = \sqrt{{\sigma_{max}}^2 + 3(\tau_{max})^2} \tag{2.39}$$

2.5.1.2. Ellipse quadrant and Ellipse arc

For ductile material, Gough and Pollard (Gough & Pollard, 1935) proposed the following ellipse quadrant equation:

$$\left(\frac{\tau_a}{\tau_{af}}\right)^2 + \left(\frac{\sigma_a}{\sigma_{af}}\right)^2 = 1 \tag{2.40}$$

For brittle material, Gough and Pollard proposed the following Ellipse Arc equation:

$$\left(\frac{\tau_a}{\tau_{af}}\right)^2 + \left(\frac{\sigma_a}{\sigma_{af}}\right)^2 \left(\frac{\sigma_{af}}{\tau_{af}} - 1\right) + \left(\frac{\sigma_a}{\sigma_{af}}\right)\left(2 - \frac{\sigma_{af}}{\tau_{af}}\right) = 1 \tag{2.41}$$

Because both Ellipse Quadrant and Ellipse Arc method use the applied stresses rather than stresses acting on the material plane, Gough's method is very simply to apply for multi-axial fatigue calculation. However, Wang et al. (Wang & Yao, 2004) proposed that Gough's method cannot be used for non-proportional loading.

2.5.1.3. Lee

In order to take into the phase difference effect into account, Lee (Lee, 1985) modified Gough's criterion as follows:

$$\sigma_{a,eq} = \sigma_a \left[1 + \left(\frac{f_{-1}\tau_a}{t_{-1}\sigma_a}\right)^{\alpha}\right]^{\frac{1}{\alpha}} / (1 - (\sigma_m/\sigma_u)^n) \tag{2.42}$$

$$\alpha = 2(1 + \beta sin\varphi) \tag{2.43}$$

2.5.2. Stress invariants

The stress invariants criterion uses the stress invariant and hydrostatic stress related parameter, which represents damage caused by shear and normal stress respectively, to calculate the multiaxial fatigue damage. For Sines et al. (Sines, Waisman, & Dolan, 1959) and Crossland (Crossland, 1956) invariant criteria, multi-axial fatigue damage is calculated through combination of second deviatoric invariant and hydrostatic stress. And the relationship between the damage caused by stress invariant and hydrostatic stress is determined by uniaxial torsion and uniaxial bending loading (Anes, Reis, Li, Fonte, & Freitas, 2014).

2.5.2.1. Crossland

Crossland (Crossland, 1956) criterion considers that multiaxial fatigue can be calculated through the combination of second deviatoric stress invariant and hydrostatic stress. Shear and normal stress amplitudes are represented by second deviatoric stress invariant and hydrostatic stress, respectively (Anes, Reis, Li, Fonte, & Freitas, 2014). The relation of second deviatoric stress invariant and hydrostatic stress is defined by following equation:

$$\left(\sqrt{J_2}\right)_a + (3\frac{\tau_{af}}{\sigma_{af}} - \sqrt{3})\sigma_{H,max} \leq \tau_{af} \tag{2.44}$$

2.5.2.2. Sines

Sines (Sines, Waisman, & Dolan, 1959) defines relationship of second deviatoric stress invariant and hydrostatic stress by fully reversed torsion and purely pulsating bending fatigue limit. Extra experiment or formula needed to determine purely pulsating axial loading fatigue limit may be the shortcoming. Sines criterion can be expressed as follows:

$$\left(\sqrt{J_2}\right)_a + (6\frac{\tau_{af}}{\sigma_{af,0}} - \sqrt{3})\sigma_{H,m} \leq \tau_{af} \tag{2.45}$$

Where $\sigma_{af,0}$ is the fatigue limit of purely pulsating axil loading, $\sigma_{H,max}$ is maximum hydrostatic stress.

2.5.2.3. Prismatic Hull

Mamiya et al. (Mamiya, Araújo, & Castro, 2009) proposed the stress invariants multiaxial criterion as follows:

$$\tau_{eq,a} + \kappa\sigma_{H,max} \leq \varsigma \tag{2.46}$$

Where $\sigma_{H,max}$ is maximum hydrostatic stress. κ and ς are material property related parameters. $\tau_{eq,a}$ stands for deviatoric stress amplitude. Note that deviatoric stress amplitude in prismatic hull method is not the same shear stress amplitude defined by critical plane method (Mamiya, Castro, Algarte, & Araújo, 2011).

The deviatoric stress tensor **X** in the space dev^3 from $\Re^3$ to $\Re^3$ can be defined by five orthonormal bases $\mathbf{B}_i$(with i=1,⋯,5) as follows:

$$\mathbf{X}(\mathrm{t}) = \sum_{i=1}^{5} x_i(t)\mathbf{B}_i \tag{2.47}$$

Five orthonormal bases are expressed as follows:

$$\mathbf{B}_1 = \frac{1}{\sqrt{6}}\begin{pmatrix} 2 & 0 & 0 \\ 0 & -1 & 0 \\ 0 & 0 & -1 \end{pmatrix}, \mathbf{B}_2 = \frac{1}{\sqrt{2}}\begin{pmatrix} 0 & 0 & 0 \\ 0 & 1 & 0 \\ 0 & 0 & -1 \end{pmatrix}$$

$$\mathbf{B}_3 = \frac{1}{\sqrt{2}}\begin{pmatrix} 0 & 1 & 0 \\ 1 & 0 & 0 \\ 0 & 0 & 0 \end{pmatrix}, \mathbf{B}_4 = \frac{1}{\sqrt{2}}\begin{pmatrix} 0 & 0 & 1 \\ 0 & 0 & 1 \\ 1 & 0 & 0 \end{pmatrix} \tag{2.48}$$

$$\mathbf{B}_5 = \frac{1}{\sqrt{2}}\begin{pmatrix} 0 & 0 & 0 \\ 0 & 0 & 1 \\ 0 & 1 & 0 \end{pmatrix}$$

$x_i(t)$ is expressed as follows:

$$\begin{aligned} x_1(\mathrm{t}) &= \sqrt{\frac{3}{2}}X_x(t) = \frac{1}{\sqrt{6}}\Big(2\sigma_x(t) - \sigma_y(t) - \sigma_z(t)\Big) \\ x_2(t) &= \frac{1}{\sqrt{2}}\Big(X_y(t) - X_z(t)\Big) = \frac{1}{\sqrt{2}}\Big(\sigma_y(t) - \sigma_z(t)\Big) \\ x_3(t) &= \sqrt{2}X_{xy}(t) = \sqrt{2}\tau_{xy}(t) \\ x_4(t) &= \sqrt{2}X_{xz}(t) = \sqrt{2}\tau_{xz}(t) \\ x_5(t) &= \sqrt{2}\mathrm{X}_{yz}(t) = \sqrt{2}\tau_{yz}(t) \end{aligned} \tag{2.49}$$

Where X_x, X_y, ⋯ are components of deviatoric tensor, while σ_x, σ_y,⋯ are components of Cauchy stress tensor (Carpinteri, Ronchei, Spagnoli, & Vantadori, 2014). **X** can be simplified as follows:

$$\mathbf{x} = [x_1\ x_2\ x_3\ x_4\ x_5]^{\mathrm{T}} \tag{2.50}$$

The half-length of prismatic hull side is expressed as follows:

$$a_i = \frac{1}{2}\Big[\max_{0\leq t<T} x_i(t) - \min_{0\leq t<T} x_i(t)\Big] \tag{2.51}$$

Deviatoric stress amplitude τ_{eq} is defined as follows:

$$\tau_{eq} = \max_{\Theta} \sqrt{\sum_{i=1}^{5} [a_i(\Theta)]^2} \tag{2.52}$$

Where Θ is the parameter used to adjust the bases $\mathbf{N}_i$ to produce maximum value in eq. (2.50).

$$a_i(\Theta) = \frac{1}{2}\left[\max_{0 \le t < T} x_i(t, \Theta) - \min_{0 \le t < T} x_i(t, \Theta)\right] \tag{2.53}$$

2.5.3. Critical plane criteria

Critical plane method can be divided into stress, strain and energy based. In this thesis, only the stress based critical plane method is considered. The procedure of applying critical plane method is basically comprised of two steps. First step is to search critical plane and second step is to use parameters such as shear and normal stress amplitudes on critical plane to calculate fatigue strength (Li, Jiang, Han, & Li, 2015).

2.5.3.1. Findley

Findley criterion (Findley, 1957) assumes shear stress amplitude is the most important factor affect multi-axial fatigue strength, and the damage caused by maximum normal stress has a linear relationship with shear stress amplitude.

Findley multiaxial fatigue criterion is expressed by following equation:

$$C_{a,eq} = C_a + kN_{max} \tag{2.54}$$

Where C_a is shear stress amplitude and N_{max} is maximum normal stress at the same material plane. Critical plane is defined as the plane which maximizes combination of C_a and N_{max}. k is material property related coefficient, which can be determined by fully reversed torsion and bending fatigue limit as follows:

$$\frac{\sigma_{af}}{\tau_{af}} = \frac{2}{1 + k/\sqrt{1 + k^2}} \tag{2.55}$$

2.5.3.2. McDiarmid

McDiarmid criterion (McDiarmid, 1994) (McDiarmid, 1991)considers two types of crack propagation; in type A, the crack propagation occurs along the surface; in case B, the crack propagation occurs into inside. Critical plane is the plane where largest shear stress amplitude acts.

McDiarmid criterion equation is expressed as follows:

$$C_{a,eq} = C_{a,max} + \frac{\tau_{A,B}}{2\sigma_u} N_{max} \tag{2.56}$$

Where τ_A is fully reversed shear stress fatigue limit for case A crack growth and τ_B for case B. σ_u is the ultimate tensile strength. For multi-axial bending and torsion loading condition, crack type A presents, $\tau_{A,B} = \tau_A = \tau_{af}$.

2.5.3.3. Matake

Matake criterion (Matake, 1977) defines the critical plane as the plane where maximum shear stress amplitude acts. Matake criterion is expressed as follows:

$$C_{a,eq} = C_{a,max} + k \cdot N_{max} \tag{2.57}$$

Where $C_{a,max}$ and N_{max} stand for shear stress amplitude and maximum normal stress on critical plane, respectively. Coefficient k can be expressed as follows:

$$k = 2\frac{\tau_{af}}{\sigma_{af}} - 1 \tag{2.58}$$

2.5.3.4. Dang Van

Dan van criterion (K, G, JF, A, & HP, 1989) assumes at stable elastic shakedown state fatigue will not occur (Karolczuk & Kluger, 2014). And the stable state can be described by mesoscopic shear stress amplitude and maximum hydrostatic stress related parameters. Critical plane is defined as the plane where maximum shear stress amplitude acts.

Dan Van criterion on the macroscopic scale used in this thesis,

$$C_{a,eq} = C_{a,max} + k \cdot \sigma_{H,max} \tag{2.59}$$

Where $\sigma_{H,max}$ is the maximum hydrostatic stress and coefficient k is defined as follows:

$$k = 3\frac{\tau_{af}}{\sigma_{af}} - \frac{3}{2} \tag{2.60}$$

2.5.3.5. Papadopoulos

Papadopoulos criterion (Papadopoulos I. V., 2001) is also a mesoscopic criterion using average shear stress amplitude. Shear stress amplitude is defined as follows:

$$\sqrt{\langle T_a \rangle} = \sqrt{5} \times \sqrt{\frac{1}{8\pi^2}\int_{\varphi=0}^{2\pi}\int_{\theta=0}^{\pi}\int_{\psi=0}^{2\pi}(T_a(\varphi,\theta,\psi)^2\, d\psi \sin(\theta) d\theta d\varphi} \tag{2.61}$$

Where angle ψ define the gliding directions. ψ and θ define material plane orientations (Anes, Reis, Li, Fonte, & Freitas, 2014). Papadopoulos (Papadopoulos I. V., 2001) defines critical plane as the plane where maximum T_a value acts. Multi-axial fatigue equation is defined as follows:

$$C_{a,eq} = \sqrt{\langle T_a \rangle} + k \cdot \sigma_{H,max} \tag{2.62}$$

Coefficient k is defined as follows:

$$k = 3\frac{\tau_{af}}{\sigma_{af}} - \sqrt{3} \tag{2.63}$$

For Biaxial loading condition, T_a can be simplified as von Mises equivalent stress (Anes, Reis, Li, Fonte, & Freitas, 2014).

For biaxial loading condition, equation (2.60) is simplified as follows:

$$C_{a,eq} = \sqrt{\frac{{\sigma_a}^2}{3} + \tau_a^2} + k \cdot \max(\frac{I_1}{3}) \tag{2.64}$$

2.5.3.6. Carpinteri-Spagnoli

Critical plane defined in C-S criterion is quite different from aforementioned multi-axial criterions. Main steps of critical plane determination for Carpinteri-Spagnoli criterion (Carpinteri, Spagnoli, & Vantadori, 2011) is quoted here:

(1) Determine averaged maximum principal stress direction.
(2) Critical plane orientation is related to direction calculated in (1).

Critical plane determination in Carpinteri-Spagnoli method is based on fracture mechanism mentioned in chapter 2.2. C-S criteria (Carpinteri & Spagnoli, 2001)modified Gough criterion as follows:

$$C_{a,eq} = \sqrt{C_a^2 + k^2 N_{a,eq}^2} \tag{2.66}$$

Where $N_{a,eq}$ stands for equivalent normal stress amplitude on critical plane. $N_{a,eq}$ is defined using Goodman mean stress correction criterion to take mean normal stress effect into account.

$$N_{a,eq} = N_a + \sigma_{af}\left(\frac{N_m}{\sigma_u}\right) \tag{2.67}$$

Where N_a stands for normal stress amplitude. N_m stands for mean normal stress. σ_u stands for material ultimate tensile strength.

Coefficient k is defined as follows:

$$k = \frac{\tau_{af}}{\sigma_{af}} \tag{2.68}$$

Fracture plane orientation determination procedure is introduced below. Maximum principal stress instantaneous direction 1 can be defined through ϕ, θ and ψ with respected to fixed *XYZ* coordinate system (Fig.2.17). Specific procedure to obtain averaged $\hat{\phi}, \hat{\theta}, \hat{\psi}$ is described in (Carpinteria, Machab, Brighentia, & Spagnoli, 1999).

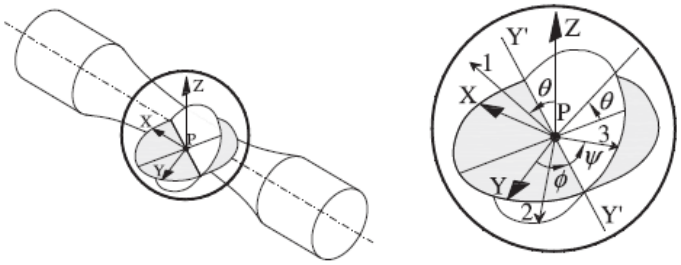

Figure. 2.17. Instantaneous principal stress directions (Carpinteri, Ronchei, Spagnoli, & Vantadori, 2014)

Carpinteria et al. (Carpinteria, Machab, Brighentia, & Spagnoli, 1999) proposes the following weighted equation to calculate averaged $\hat{\phi}, \hat{\theta}, \hat{\psi}$:

$$\hat{\phi} = \frac{1}{W}\int_0^T \phi(t)W(t)dt \quad \hat{\theta} = \frac{1}{W}\int_0^T \theta(t)W(t)dt \quad \hat{\psi} = \frac{1}{W}\int_0^T \psi(t)W(t)dt$$
$$W = \int_0^T W(t)dt \tag{2.69}$$

Where T is loading cycle period. Weight function $W(t)$ is originally defined as:

$$\mathrm{W(t)} = \begin{cases} 0 & if\ \sigma_1(t) \geq c\sigma_{af} \\ \left(\frac{\sigma_1(t)}{c\sigma_{af}}\right)^m \sigma & if\ \sigma_1(t) \geq c\sigma_{af} \end{cases} \qquad 0 < c \leq 1 \tag{2.70}$$

Where σ_1 is the maximum principal stress.

In order to simplify the lengthy procedure for getting averaged Euler angles $\hat{\phi}, \hat{\theta}$ and $\hat{\psi}$, Carpinteri et al. (Carpinteri, Spagnoli, & Vantadori, 2011) use instantaneous direction of maximum σ_1 axes as average weighted direction. Simplified averaged weighted equation is defined as follows:

$$\mathrm{W(t)} = H\ \left[\sigma_1(t) - \sigma_{1,max}\right] \begin{matrix} H[x] = 1\ for\ x \geq 0 \\ H[x] = 0\ for\ x < 0 \end{matrix} \tag{2.71}$$

Where $\sigma_{1,max}$ is maximum value of maximum principal stress σ_1.

Although simplified weighted equation is relative easy to apply compared to original weighted equation, simplified weighted equation cannot take into material property into account, which is the disadvantage.

The algorithm to calculate stress amplitude C_a on the critical plane using prismatic hull method for Carpinteri-Spagnoli multi-axial fatigue criterion is listed below (Mamiya, Castro, Algarte, & Araújo, 2011):

(1). Calculate the stress history $\{\boldsymbol{\sigma}(t), t = 1{:}\,T\}$ on the critical plane:

(2). Set C_a=0;

(3). For $\theta = 0{:}\,\Delta\theta{:}\frac{\pi}{2}$

(3.1). Calculate the stress history in a θ-oriented basis $(\mathrm{C}_u(\theta), \mathrm{C}_v(\theta))$

$$\begin{pmatrix} \mathrm{C}_u(t,\theta) \\ \mathrm{C}_v(t,\theta) \end{pmatrix} = \begin{bmatrix} cos\theta & sin\theta \\ -sin\theta & cos\theta \end{bmatrix} \begin{pmatrix} \mathrm{C}_u(t) \\ \mathrm{C}_v(t) \end{pmatrix} \tag{2.72}$$

(3.2). Calculate half-lengths of θ-oriented prismatic hull sides $\mathrm{C}_{u,a}(\theta)$ and $\mathrm{C}_{u,a}(\theta)$

$$\mathrm{C}_{u,a}(\theta) = \frac{1}{2}\left[\max_{0\leq t<T} C_u(t,\theta) - \min_{0\leq t<T} C_u(t,\theta)\right] \tag{2.73}$$

$$\mathrm{C}_{v,a}(\theta) = \frac{1}{2}\left[\max_{0\leq t<T} C_v(t,\theta) - \min_{0\leq t<T} C_v(t,\theta)\right] \tag{2.74}$$

(3.3). Calculate half diagonal length of θ-oriented prismatic hull:

$$\mathrm{C}_a(\theta) = \sqrt{\mathrm{C}_{u,a}(\theta)^2 + \mathrm{C}_{v,a}(\theta)^2} \tag{2.75}$$

(3.4). If $\mathrm{C}_a(\theta) > \mathrm{C}_a$, set $\mathrm{C}_a = \mathrm{C}_a(\theta)$;

End.

3. Proposed PDMR based method

The proposed PDMR is defined in 3D $N - C_u - C_v$ space. In order to compare with modified C-S criterion, same Goodman mean normal stress correction is used. Proposed method will also apply Smith-Watson-Topper mean normal stress correction method to access mean normal stress correction effect. Equivalent shear stress amplitude is expressed as follows:

$$C_{a,eq} = \sqrt{C_{ua}^2 + C_{va}^2 + k^2 N_{a,eq}^2} \tag{3.1}$$

$$N_{a,eq} = N_a + \sigma_{af}\left(\frac{N_m}{\sigma_u}\right) \tag{3.2}$$

Coefficient k in the equation (3.1) is calculated from the equation below:

$$\mathrm{k} = \frac{\tau_{af}}{\sigma_{af}} \tag{3.3}$$

The proposed method define critical plane relative to fracture plane the same as Carpinteri-Spagnoli method. Two fracture plane orientation determination methods based on observation of plotted equivalent stress amplitude on each plane calculated by PDMR in 3D $N - C_u - C_v$ space.

First proposed method define the material plane where maximum equivalent stress amplitude acts as fracture plane using following equation:

$$C_{a,eq} = \sqrt{C_{ua}^2 + C_{va}^2 + N_{a,eq}^2} \tag{3.4}$$

$$N_{a,eq} = N_a + \sigma_{af}\left(\frac{N_m}{\sigma_u}\right) \tag{3.5}$$

Both the proposed first fracture plane orientation determination method and modified average maximum principal stress direction method (Carpinteri, Spagnoli, & Vantadori, 2011) define fracture plane without material property taken into account, which is the drawback compared to the following proposed second method.

The second proposed method can be described as a max-min optimization procedure using the equation (3.1).

a) At every φ angle, search ϑ^* to get the maximum equivalent stress amplitude defined by PDMR method.

b) At the determined ϑ^* angle, search φ^* in the interval $\varphi \in [0, \pi]$ to get the minimum equivalent stress amplitude. The angle between longitudinal axis and normal vector to fracture plane is defined as $\left|\varphi^* - \frac{\pi}{2}\right|$.

In order to evaluate the coefficient k effect, the third proposed method defined the coefficient as constant $\sqrt{3}$ and same searching procedure as the second method.

4. Validation

4.1 Fracture plane orientation

The experimental synchronous loading data (APPENDIX A) collected by Carpinteri et al. in (Carpinteri A. , Brighenti, Macha, & Spagnoli, 1999) is examined in this chapter to validate the feasibility of the two proposed fracture plane orientation determination methods. The fracture plane orientation calculated by the two proposed methods and modified average maximum principal stress direction method are provided in APPENDIX A.

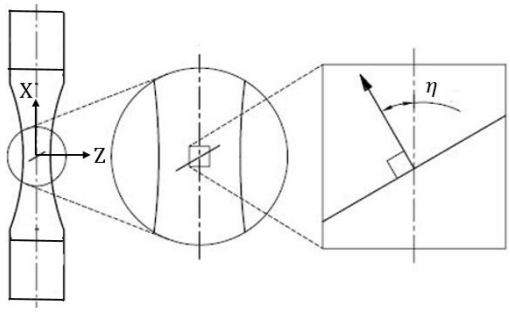

Figure 4.1. angle η to define fracture plane orientation

For uniaxial torsion, uniaxial tension and combined non-proportional torsion-tension loading (APPENDIX A), loading histories, stress paths on the fracture plane in the 3D coordinate and equivalent shear stress amplitudes on each material plane are shown below for the purpose of illustration:

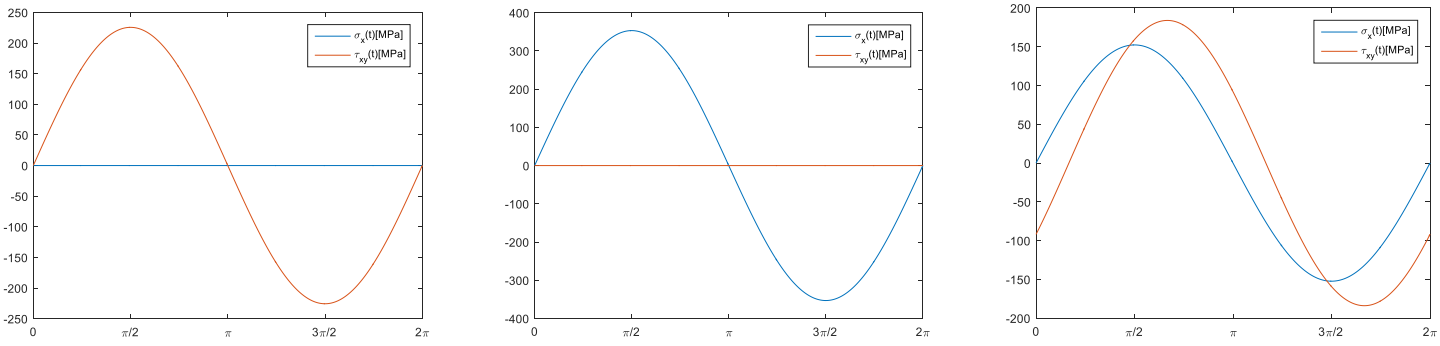

Figure 4.2. Loading histories for tests 1, 9 and 11

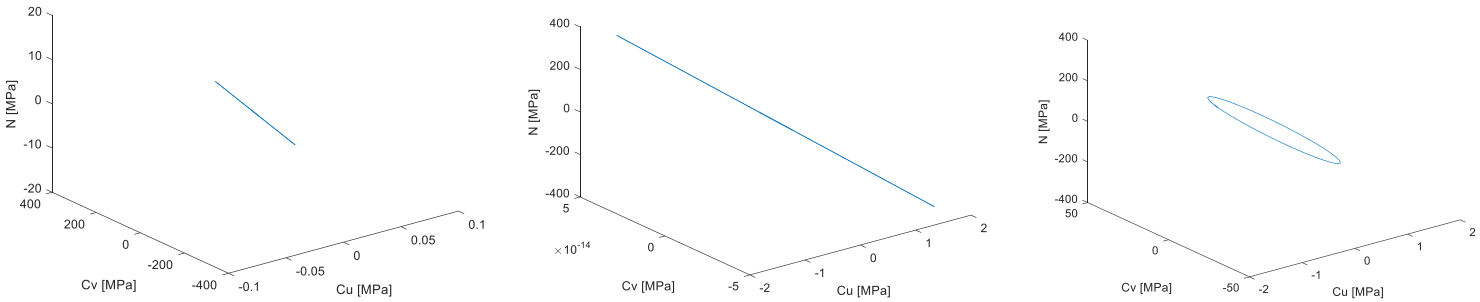

Figure 4.3. Stress paths on the fracture plane based on proposed first method for tests 1, 9 and 11

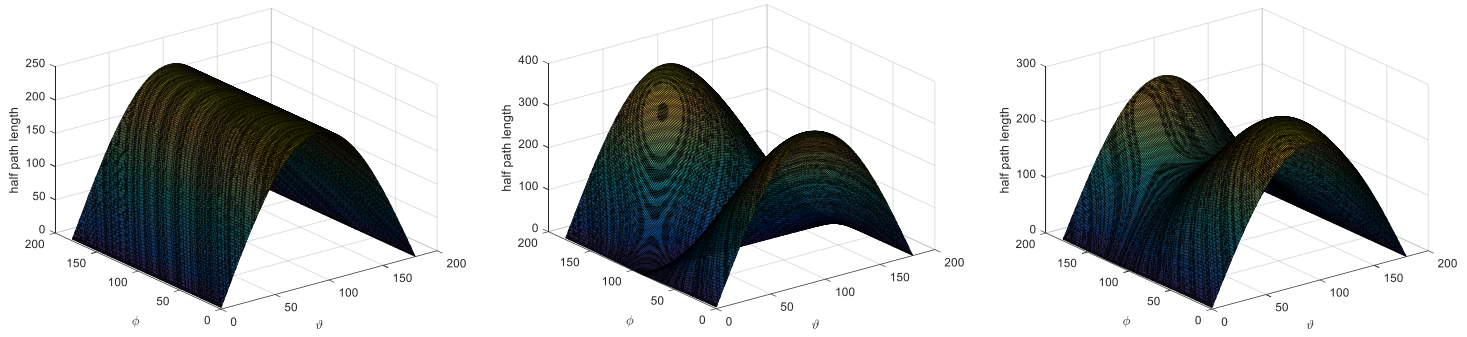

Figure 4.4. Equivalent shear stress amplitudes on each material plane based on proposed first method for tests 1, 9 and 11

The same tests are calculated by applying second proposed methods, stress paths on the fracture plane in the 3D coordinate and equivalent shear stress amplitudes on each material plane are shown below for the purpose of comparison.

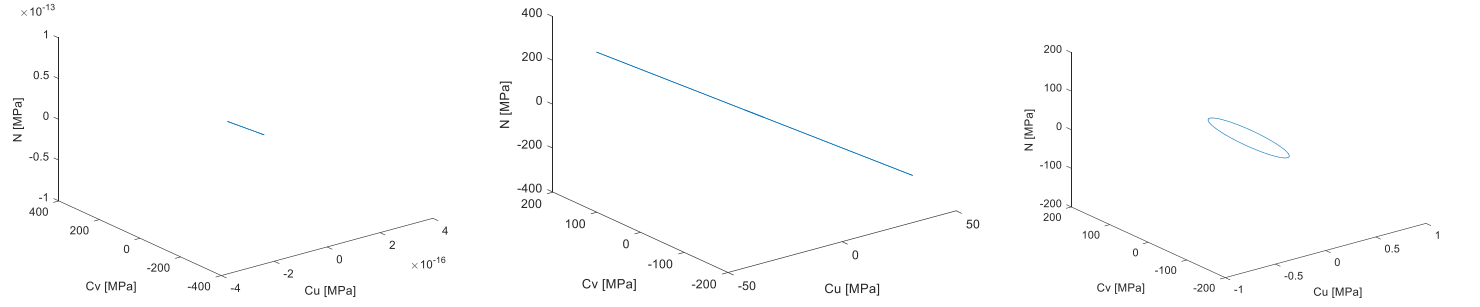

Figure 4.5. Stress paths on the fracture plane based on proposed second method for tests 1, 9 and 11

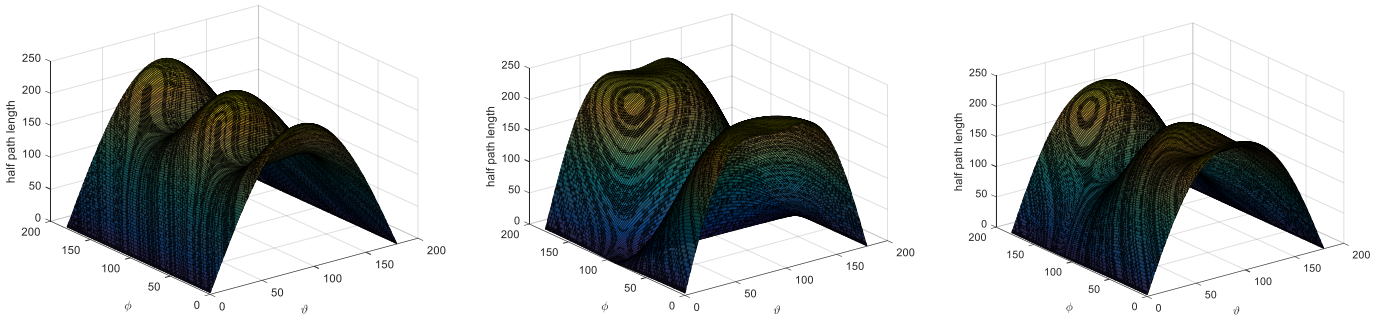

Figure 4.6. Equivalent shear stress amplitudes on each material plane based on proposed second method for tests 1, 9 and 11

Fracture plane orientation results from the experiment (Carpinteri A. , Brighenti, Macha, & Spagnoli, 1999) and (Carpinteri & Spagnoli, 2001) and estimation by applying CS and proposed methods are shown in Figure 4.7 for the purpose of comparison.

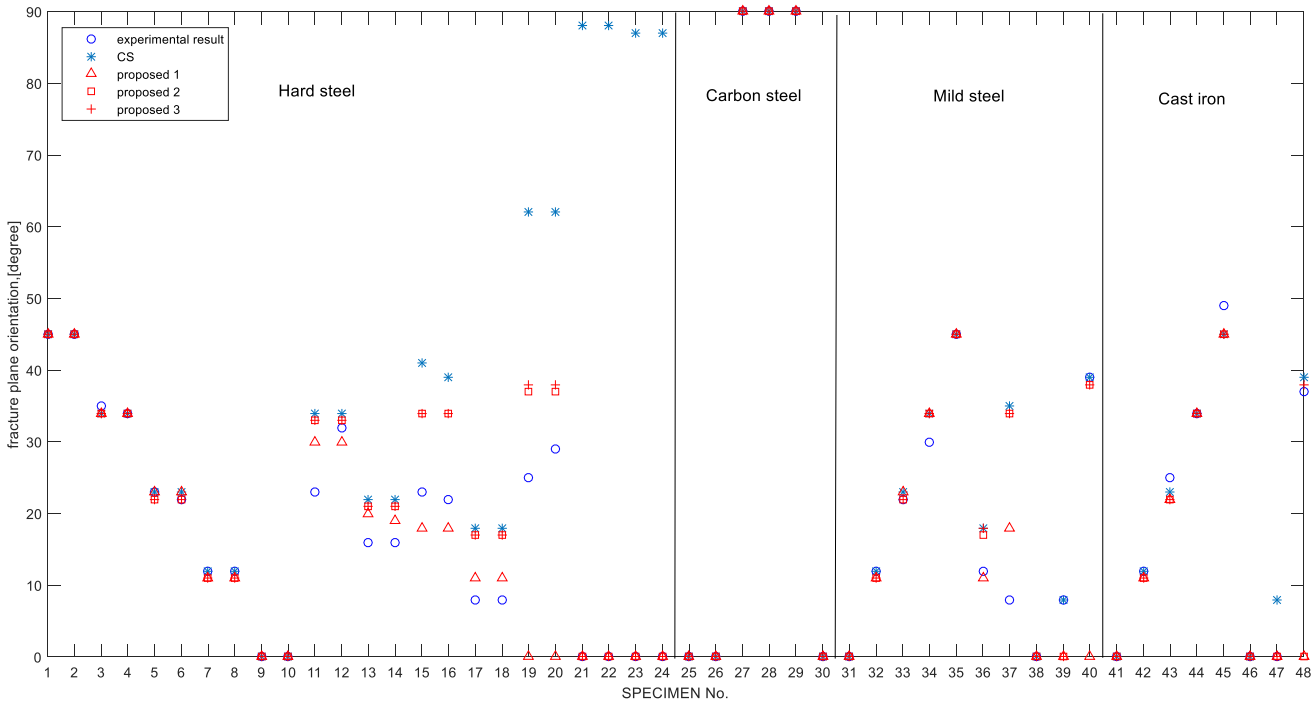

Fig.4.7. Fracture plane orientation result from the experiment and the estimation by applying CS average maximum principal stress method and two proposed methods

As can be seen from Figure 4.7, all the methods can give almost the same predations as the experimental results for test 1-10&25-28&31-35&41&45 which correspond to proportional loading and test 29&30 which correspond to180 degree out-of-phase loading for hard steel, carbon steel, mild steel

and cast iron. The C-S fracture plane orientation determination method gives very bad estimation for large out-of-phase loading, such as tests19-24 which correspond to 90 degree out-of-phase loading, while the proposed methods can give satisfy estimation, especially the proposed 3 method. The fracture plane orientation estimated by proposed 2 and 3 are almost the same except test 48 corresponding to cast iron under 90 out-of-phase loading condition. Overall, the results given by proposed 3 agrees very well with experimental results.

4.2 Results of PDMR based method

Experimental data corresponding to fatigue limit conditions is examined in this chapter to validate the proposed method. Experimental data (APPENDIX B and C) examined here are collected by Carpinteri et al. (Carpinteri, Ronchei, Spagnoli, & Vantadori, 2014) from published literature about bars and tubes under various loading types.

Fatigue properties of the experiment components is provided in APPENDIX B. Multi-axial stress states corresponding to fatigue limit are provided in APPENDIX C (where $\lambda_{xy} = \omega_{xy}/\omega_x$ or $\lambda_y = \omega_y/\omega_x$). Critical plane orientation defined by angle γ between normal vector **w** to critical plane and specimen's longitudinal axis X is also provided in the APPENDIX C.

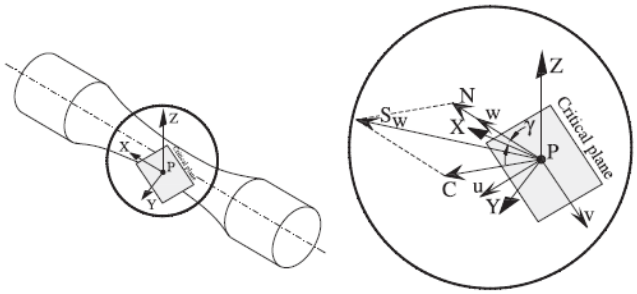

Fig.4.8. angle γ used to define the critical plane (Carpinteri, Ronchei, Spagnoli, & Vantadori, 2014)

The effective stress range defined by the path-dependent maximum range method is composed of real path and virtual path. The virtual path is the imaginary stress path and not composed of stress path on critical plane. In order to access virtual path effect in the multi-axial fatigue strength estimation, the modified PDMR with only the real stress path is proposed to compare with the original PDMR method.

58 tests (APPENDIX C) can be divided into two groups. The first group (tests 1-50), loading histories are synchonous and stress paths on the critical plane in 3D $N - C_u - C_v$ space is either line or ellipse, there are no vritual path accoridting to the PDMR method, so the proposed real path PDMR method will get exactly the same result as the original PDMR method. The second group (tests 51-58), the stress loadings are asynchonous, there are virtual paths on the critical plane in 3D $N - C_u - C_v$ space and the two PDMR methods are expected to give different results.

4.2.1 PDMR real path based method

Load histories, stress path in the 3D $N - C_u - C_v$ space and the equivalent shear stress amplitudes on each material plane of some synchronous loading tests are shown in figure below for the purpose of illustration.

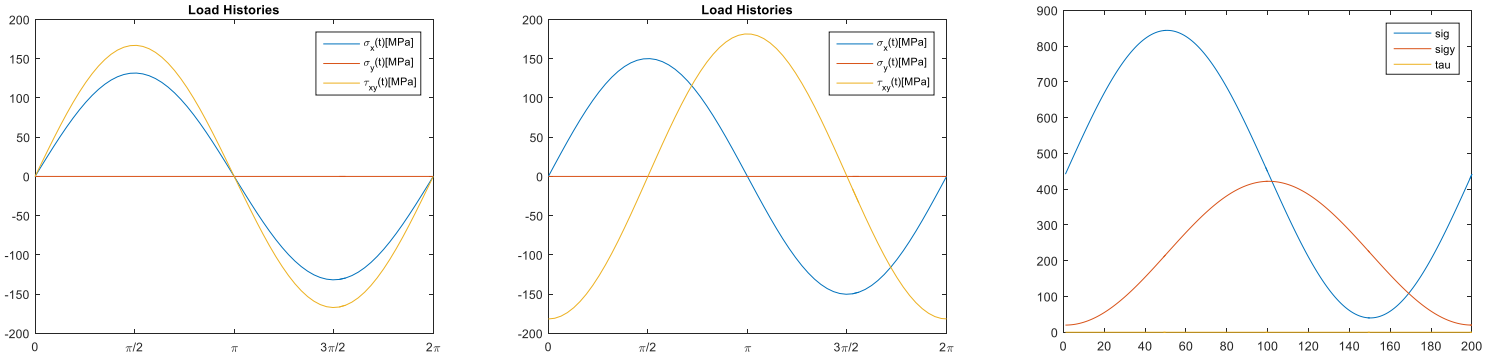

Fig.4.9 Load histories for synchronous data (tests 1, 13 and 31)

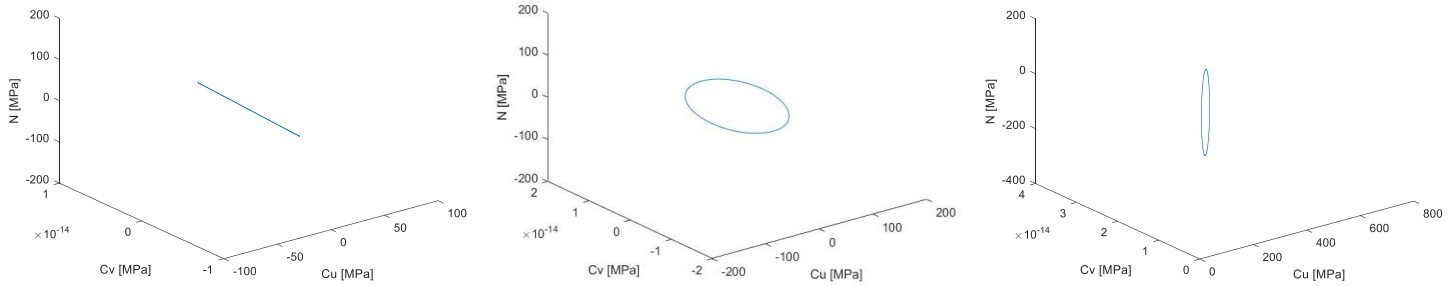

Figure 4.10. Stress paths on the critical plane (tests 1, 13 and 31)

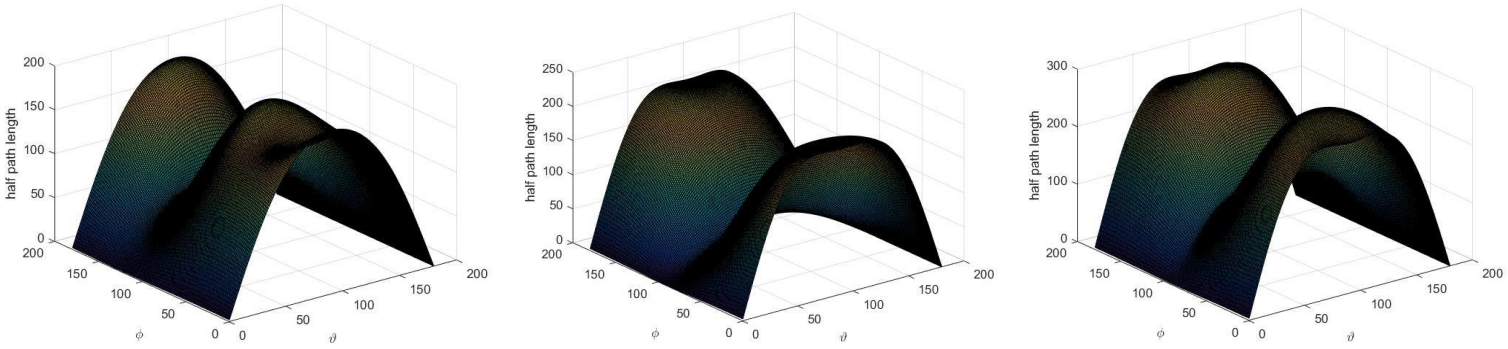

Figure 4.11. Equivalent shear stress amplitudes on each plane (tests 1, 13 and 31)

Load histories, stress path in 3D $N - C_u - C_v$ space and the equivalent shear stress amplitudes on each plane of some asynchronous loading tests are shown in figure below for the purpose of illustration.

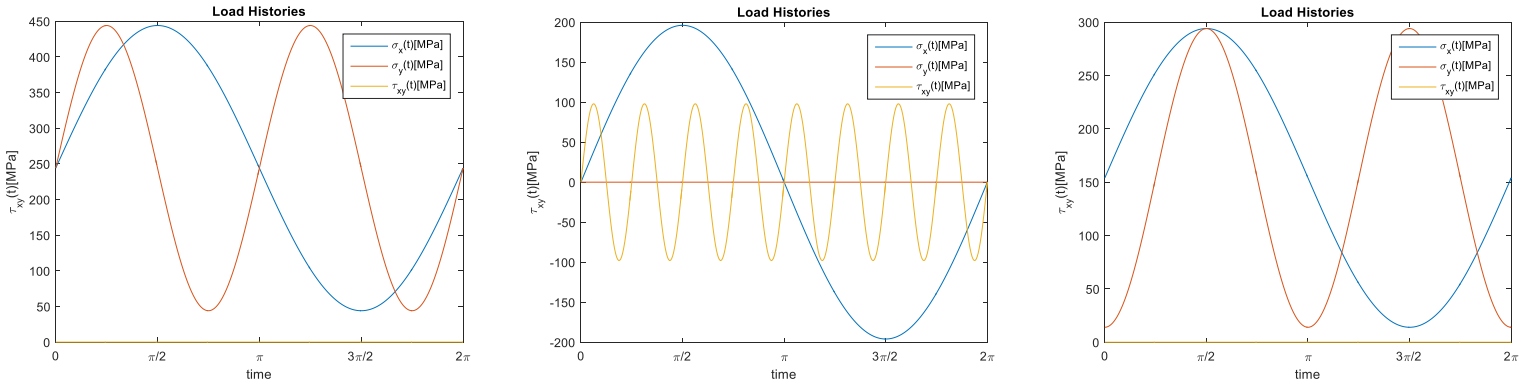

Fig.4.12. Load histories for asynchronous data (tests 51, 55 and 58)

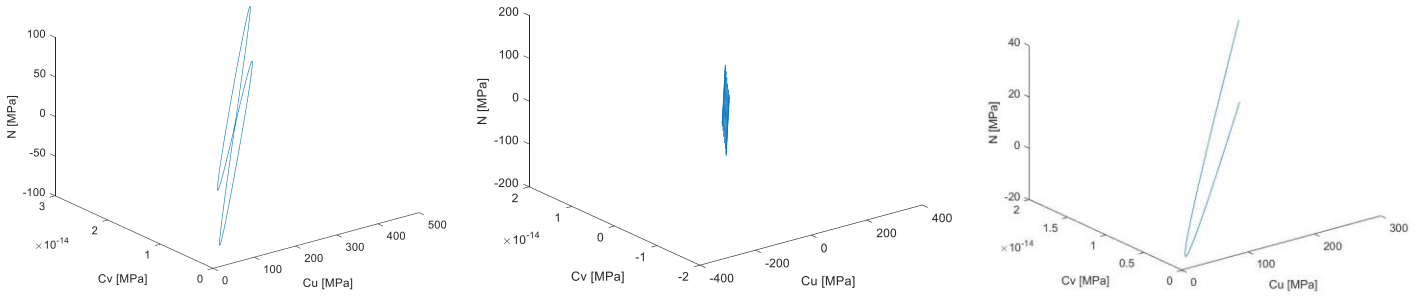

Figure 4.13. Stress paths on the critical plane (tests 51, 55 and 58)

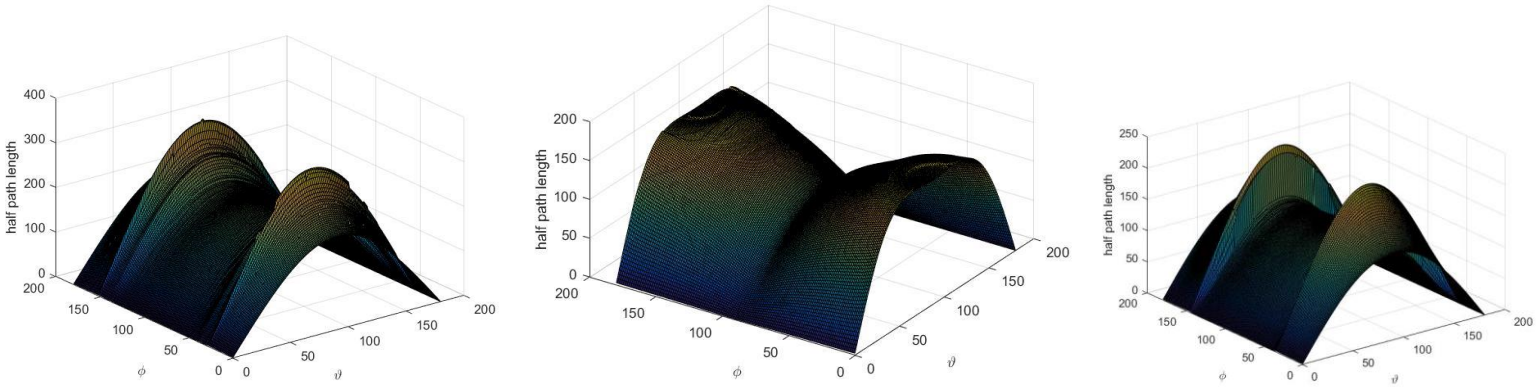

Figure 4.14. Equivalent shear stress amplitudes on each plane (tests 51, 55 and 58)

4.2.2 PDMR based method

Load histories, stress path in the 3D $N - C_u - C_v$ space and the equivalent shear stress amplitudes on each plane of same asynchronous loading tests used in 4.3.1 are shown in figure below for the purpose of illustration.

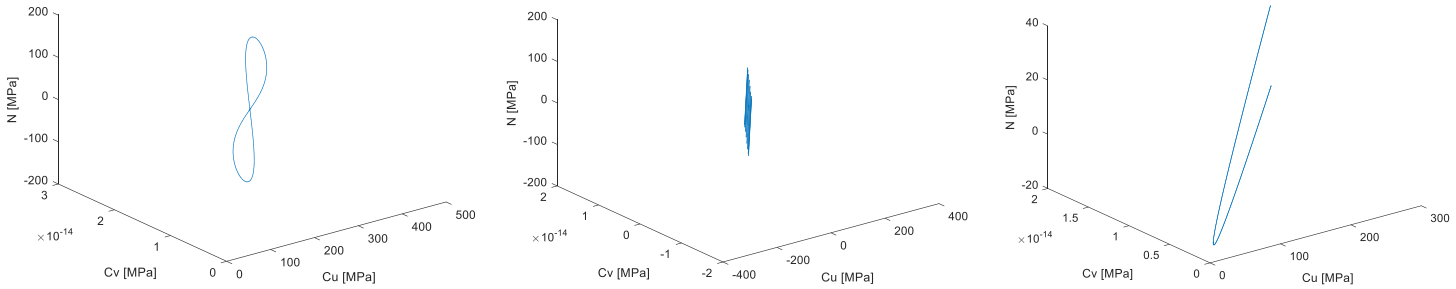

Figure 4.15. Stress paths on the critical plane (tests 51, 55 and 58)

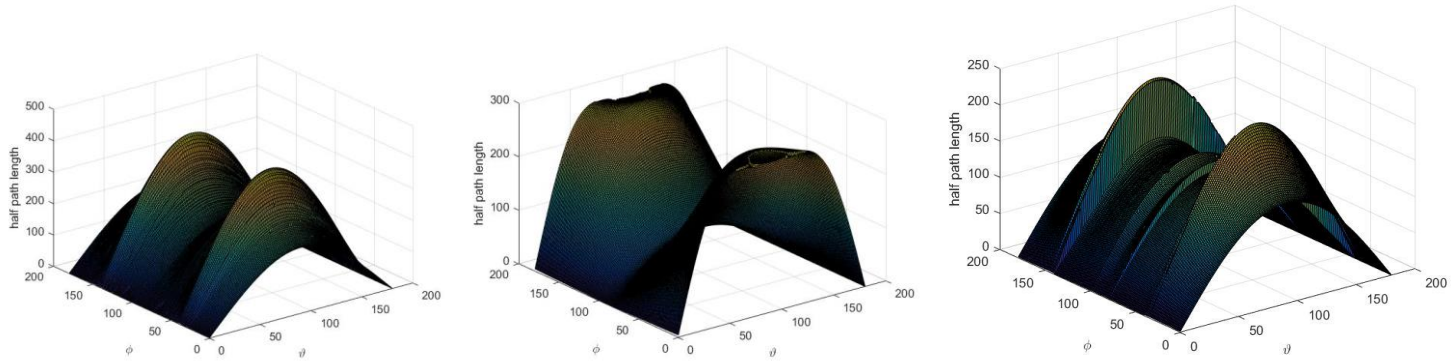

Figure 4.16. Equivalent shear stress amplitudes on each plane (tests 51, 55 and 58)

Error index is introduced to evaluate fatigue strength estimation:

$$I\% = \frac{C_{a,eq} - \tau_{af}}{\tau_{af}} 100\% \tag{4.1}$$

Where $C_{a,eq}$ is equivalent shear stress amplitude. τ_{af} stands for fully reversed shear stress fatigue limit. Positive values of *I* indicates multiaxial criteria conservatively estimates fatigue strength compared to experimental results. The values of error index for each test calculated by applying modified Carpinteri-Spagnoli criteria using PH method and proposed two PDMR methods is plotted in figure 4.17. As can be seen from the Figure 4.17, the C-S method tends to give non-conservative results except the extremely hard ($\tau_{af}/\sigma_{af} \geq 0.9$)material (tests 7-9 and 25-28) which have no obvious non-proportional loading effect (Wei & Dong, 2010). The proposed PDMR based critical plane method also give conservative estimation for the extremely hard material. It makes sense since the PDMR method is originally proposed for ductile material which has obvious non-proportional loading effect (Wei & Dong, 2010). It is expected that the proposed PDMR method will overestimate the fatigue strength for the cast materials. Although the proposed fracture plane orientation determination method and the critical plane correlation equation considering the material property, the proposed method cannot fully reflect the non-proportional insensitivity effect for cast material.

For tests 1-10 which correspond to proportional loading without mean stress, all the methods get approximately the same results. For tests 38-50 which correspond to large out-of-phase loading,

because the proposed PDMR based methods tends to estimate larger critical plane angle γ (APPDENDIX D) with respected to the modified C-S method, the proposed PDMR based methods produce less non-conservative results and improve the estimation with respect to modified Carpinteri-Spagnoli methods.

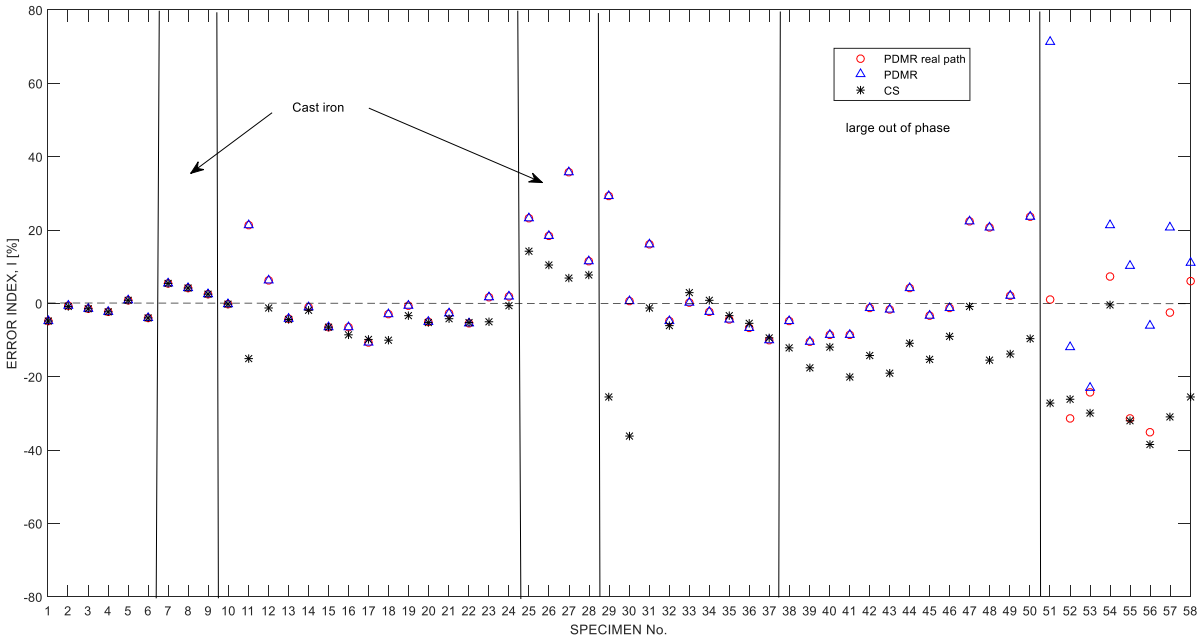

Fig.4.17. Error index values computed via modified C-S and two proposed PMDR methods

In order to access the material property effect for the proposed PDMR based methods, 58 tests are divided into mild steel ($\tau_{af}/\sigma_{af} \leq 0.6$), hard steel ($0.6 < \tau_{af}/\sigma_{af} < 0.9$) and extremely hard steel($\tau_{af}/\sigma_{af} \geq 0.9$). Error index calculated by real path PDMR based method for different material property are provided in Figure below. Error index in the range of $\pm$10% accounts for 65%, 80% and 60% for mild steel, hard steel and extremely steel respectively.

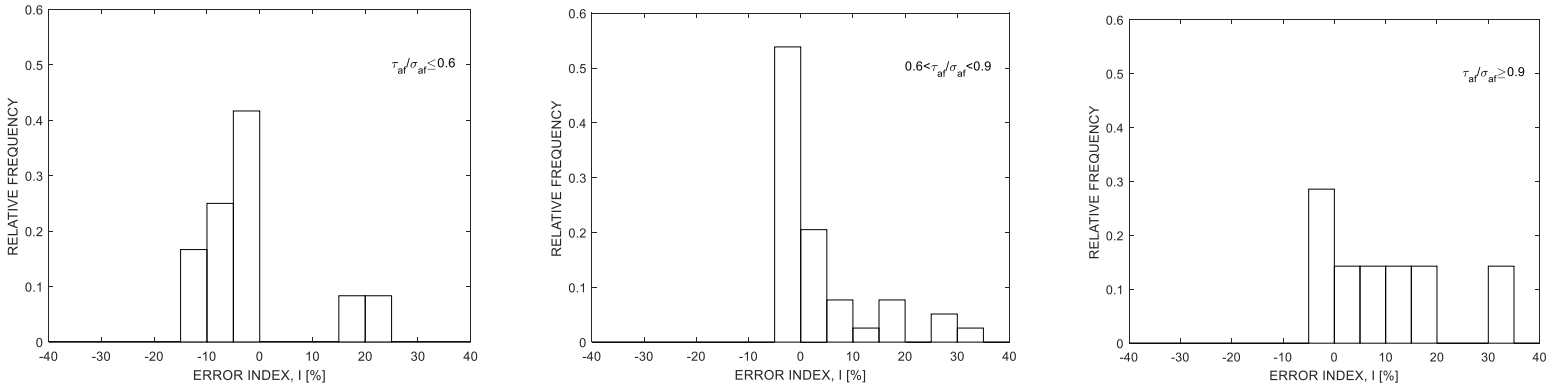

Fig.4.18. Error index for different material property

In order to compare with other critical plane methods, two parameters are introduced.

Mean value of the error index $\mu_{I\%}$ is expressed in (4.2)

$$\mu_{I\%} = \frac{1}{n}\sum_{i=1}^{n} I\%_i \tag{4.2}$$

The sample standard deviation of the error index $s_{I\%}$ is expressed in (4.3)

$$s_{I\%} = \sqrt{\frac{1}{n-1}\sum_{i=1}^{n}(I\%_i - \mu_{I\%})} \tag{4.3}$$

Error index calculated by various critical plane methods is shown in figure 4.22. The proposed PDMR based method with SWT mean normal stress correction is also calculated to assess mean stress modification effect.

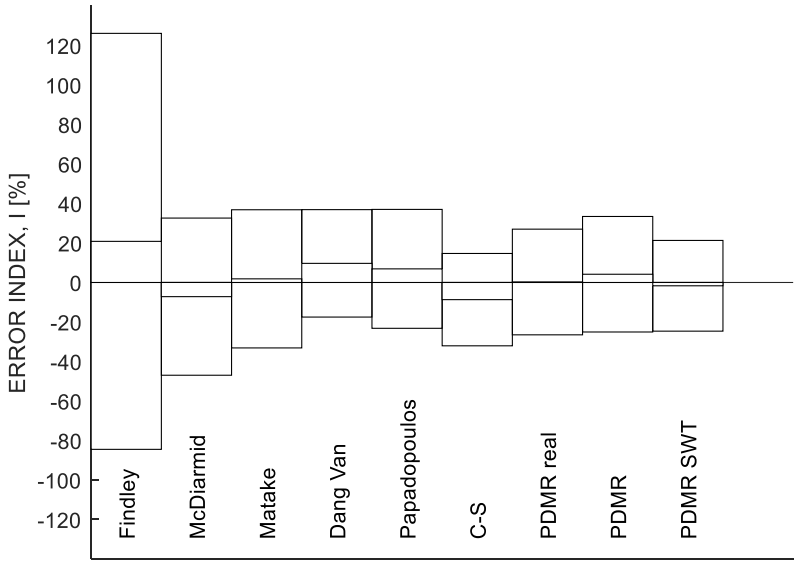

Fig.4.19. Error index calculated by various critical plane methods

As can be seen from the figure above, proposed PDMR based methods give good estimation results compared to another methods introduced in 2.5.

4.3 Stress cycle from industry

A variable amplitude stress cycle from industry (Bruun, 2013) will be assessed according to aforementioned critical plane methods. The experiment component is assumed to be Stahl ausser diesen and material parameter is given at APPENDIX B. There are 142 steps in one cycle. The stress cycly is normalize by the maximum stress σ_x.

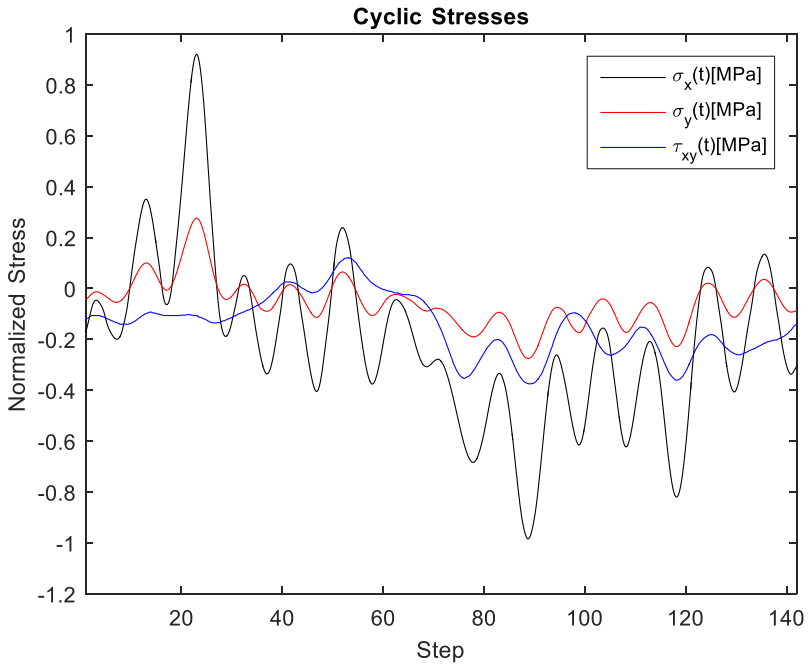

Fig.4.20. Stress history

Table 4.1 normalize equivalent stress amplitude calculated by various method.

Value	Findley	McDiarmid	Matake	Dang Van	Papadopoulos	PDMR real	PMDR
γ	23	44	44	44	89	43	49
Equivalent amplitude	0.55	0.55	0.55	0.60	0.53	0.59	0.59

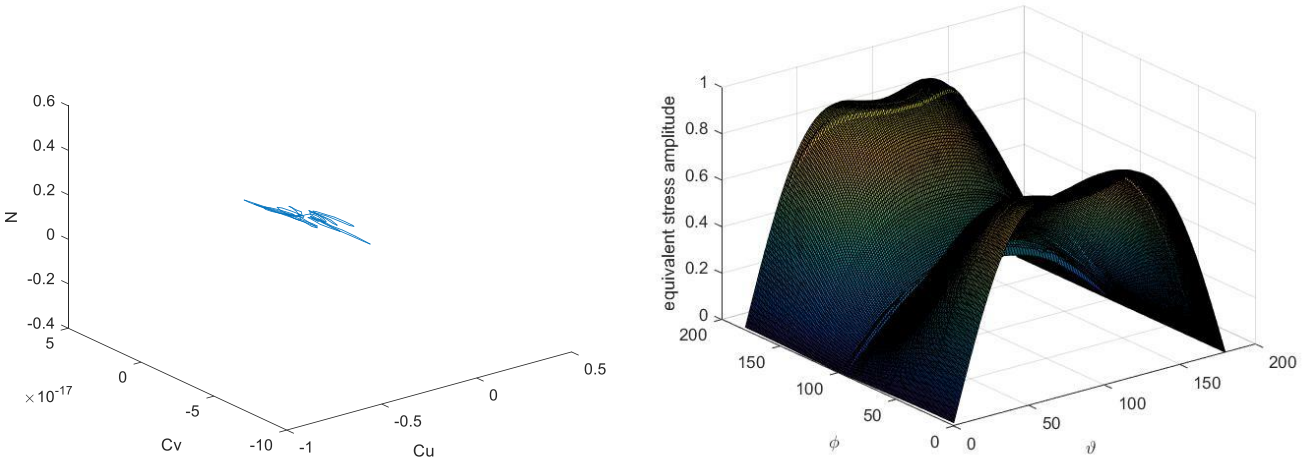

Fig.4.21. Stress path and equivalent stress amplitude on each plane

4.4 Fatigue life prediction

Fatigue life will also be predicted by the proposed method based on nominal stress. All the experimental results collected by (SUSMEL & TOVO, 2004)are circular tube-to-plate welded joints under tension, torsion, proportional or non-proportional combined tension and torsion loading.

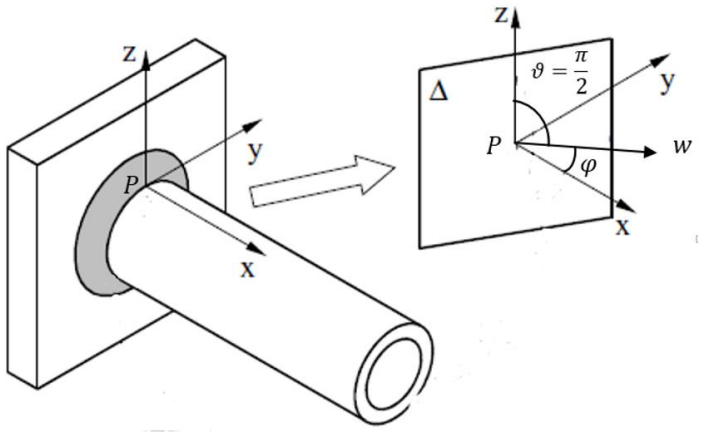

Fig.4.22.Joint Geometry

The parameter normal stress fatigue limit σ_{af} , shear stress fatigue limit τ_{af} , reverse slope value of normal stress *S-N* curve m and reverse slope value of shear stress *S-N* curve m^*calculated by (SUSMEL & TOVO, 2004) is provided in Appendix E. The loading paths is provided in figure 4.23.

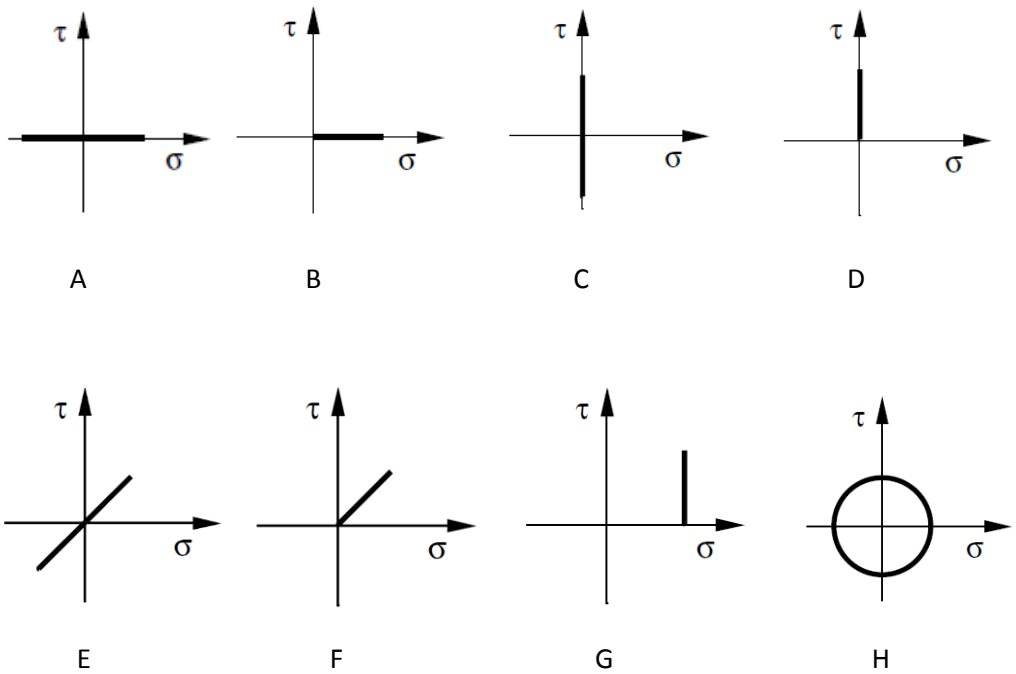

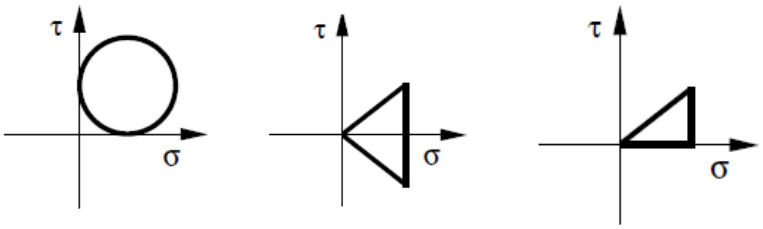

I J K

Figure 4.23: Loading paths

Basquin equation is used to relate the fatigue life N_f under stress amplitude σ_a and reference fatigue life N_{af} under fully reversed normal stress σ_{af}.

$$\sigma_a = \sigma_{af}(\frac{N_{af}}{N_f})^{\frac{1}{m}} \tag{4.4}$$

The same relationship can be applied to shear stress.

$$\tau_a = \tau_{af}(\frac{N_{af}}{N_f})^{\frac{1}{m^*}} \tag{4.5}$$

Substitute the equation (4.4) and (4.5) to (3.1) and (3.2) to get the following equation.

$$\sqrt{\left(N_a + \sigma_{af}(\frac{N_{af}}{N_f})^{\frac{1}{m}}\left(\frac{N_m}{\sigma_u}\right)\right)^2 + \left(\frac{\sigma_{af}}{\tau_{af}}\right)^2 \left(\frac{N_{af}}{N_f}\right)^{\frac{2}{m}} \left(\frac{N_f}{N_{af}}\right)^{\frac{2}{m^*}} C_a^2} = \sigma_{af}\left(\frac{N_{af}}{N_f}\right)^{\frac{1}{m}} \tag{4.6}$$

N_f is calculated by means of iteration.

Also the following equation with constant k is used to evaluate the coefficient effect.

$$\sqrt{\left(N_a + \sigma_{af}\left(\frac{N_m}{\sigma_u}\right)\right)^2 + \left(\frac{\sigma_{af}}{\tau_{af}}\right)^2 C_a^2} = \sigma_{af}\left(\frac{N_{af}}{N_f}\right)^{\frac{1}{m}} \tag{4.7}$$

The experimental fatigue life and predicted fatigue life by the equation (4.5) and (4.6) are showed in figure below.

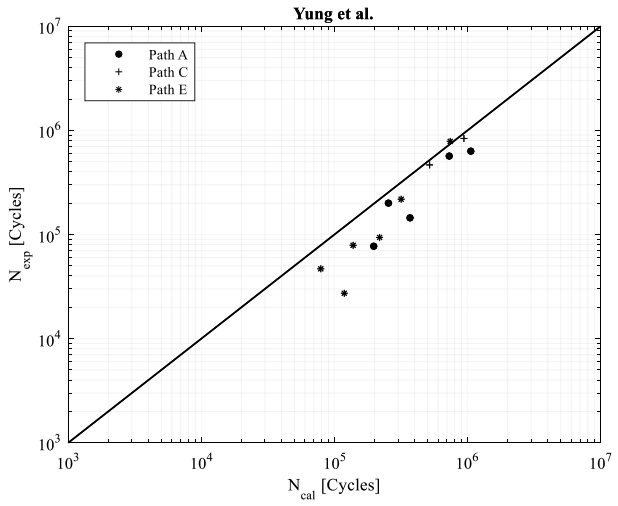
Yung et al.
Path A
Path C
Path E
N exp [Cycles]
N cal [Cycles]

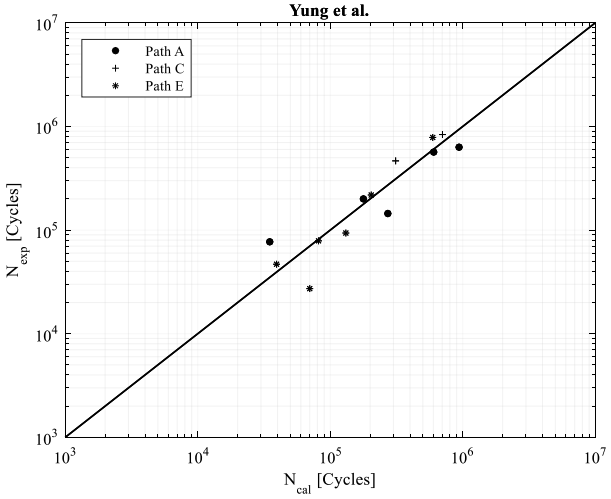
Yung et al.
Path A
Path C
Path E
N exp [Cycles]
N cal [Cycles]

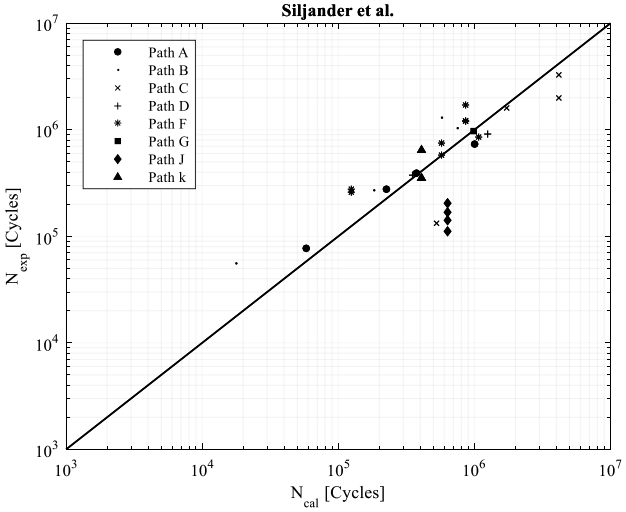
Siljander et al.
Path A
Path B
Path C
Path D
Path F
Path G
Path J
Path k
N exp [Cycles]
N cal [Cycles]

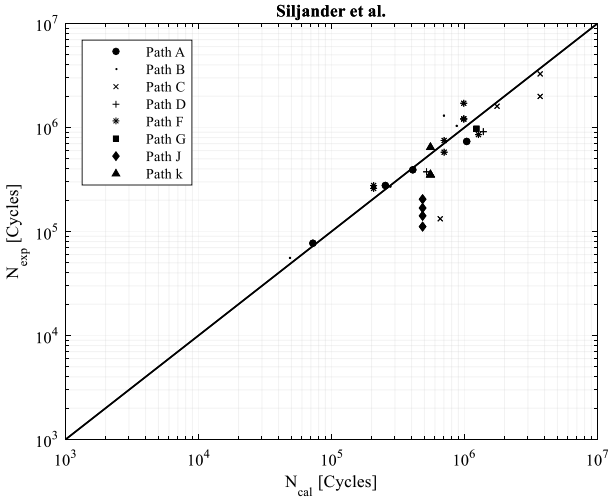
Siljander et al.
Path A
Path B
Path C
Path D
Path F
Path G
Path J
Path k
N exp [Cycles]
N cal [Cycles]

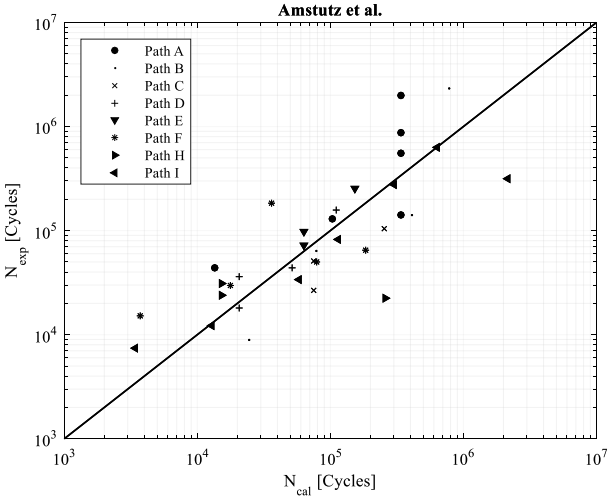
Amstutz et al.
Path A
Path B
Path C
Path D
Path E
Path F
Path H
Path I
N exp [Cycles]
N cal [Cycles]

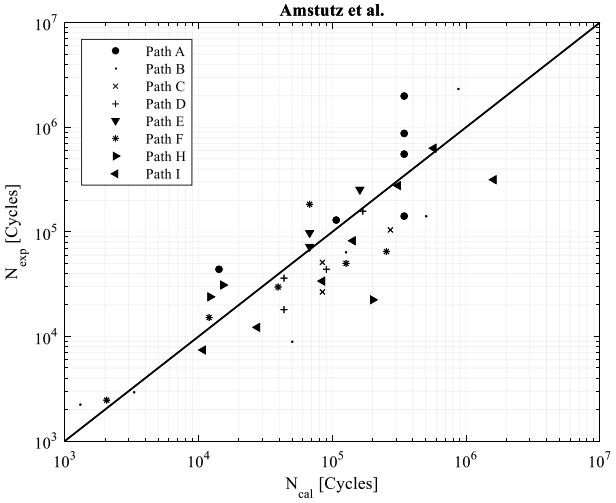
Amstutz et al.
Path A
Path B
Path C
Path D
Path E
Path F
Path H
Path I
N exp [Cycles]
N cal [Cycles]

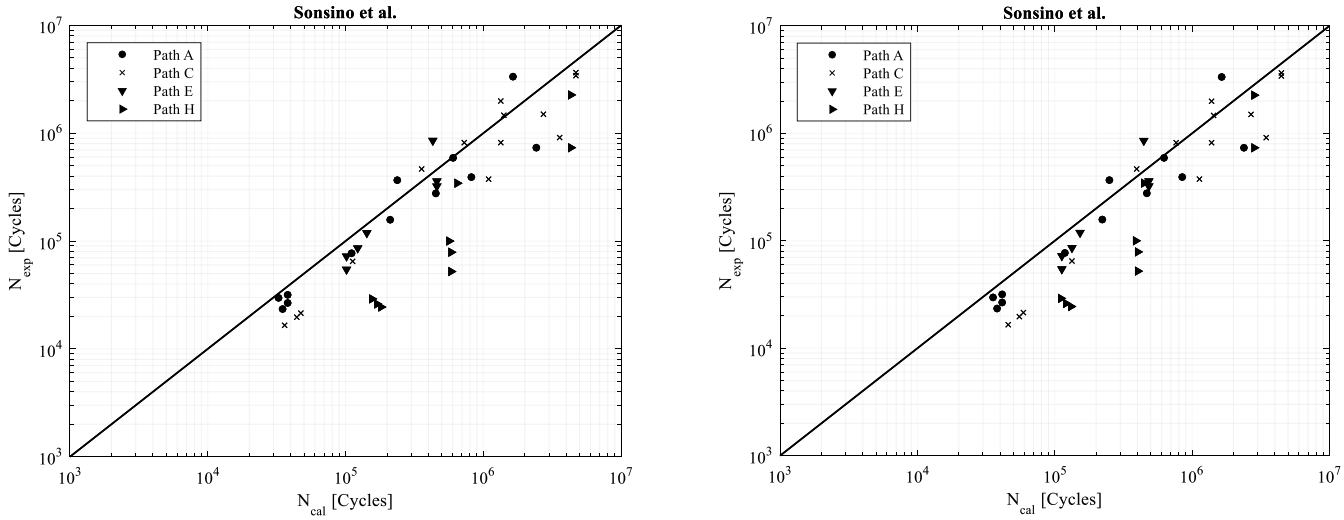

a) b)

Fig.4. 24 Experimental cycles to failure and predicted cycles to failure with a) iteration method and b) constant coefficient method

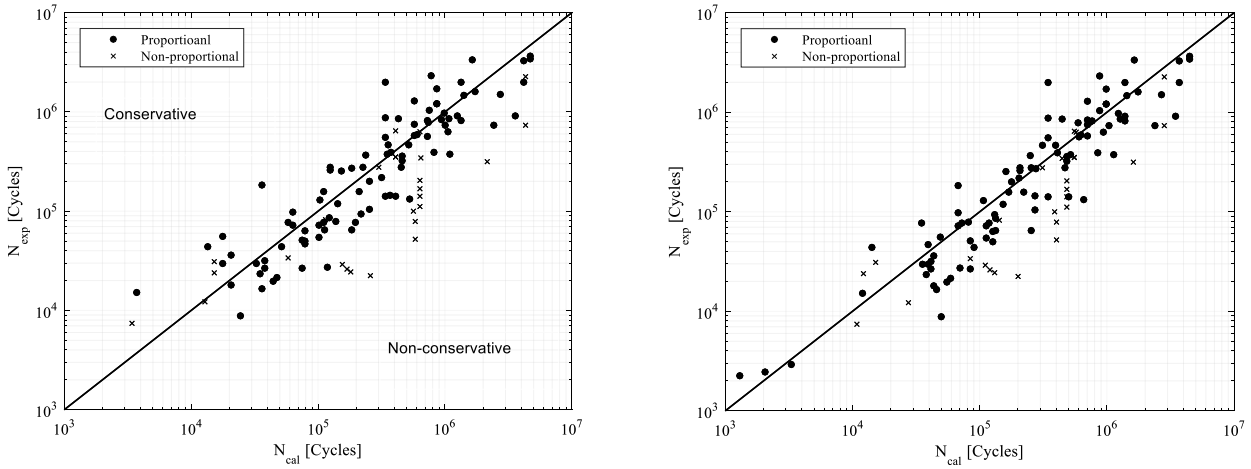

Fig.4. 25 Experimental cycles to failure and predicted cycles to failure for all data with a) iteration method and b) constant coefficient method

As can be seen from the figure above, satisfied estimation can be made by proportional data. But for non-proportional loading, the proposed method tends to give non-conservative estimation.

Error index is introduced to evaluate the fatigue life estimation.

$$I(\%) = \begin{cases} \dfrac{N_{exp} - N_{cal}}{N_{exp}} 100 \; for \; N_{cal} \leq N_{exp} \\ \dfrac{N_{exp} - N_{cal}}{N_{cal}} \; 100 \; for \; N_{cal} > N_{exp} \end{cases} \tag{4.7}$$

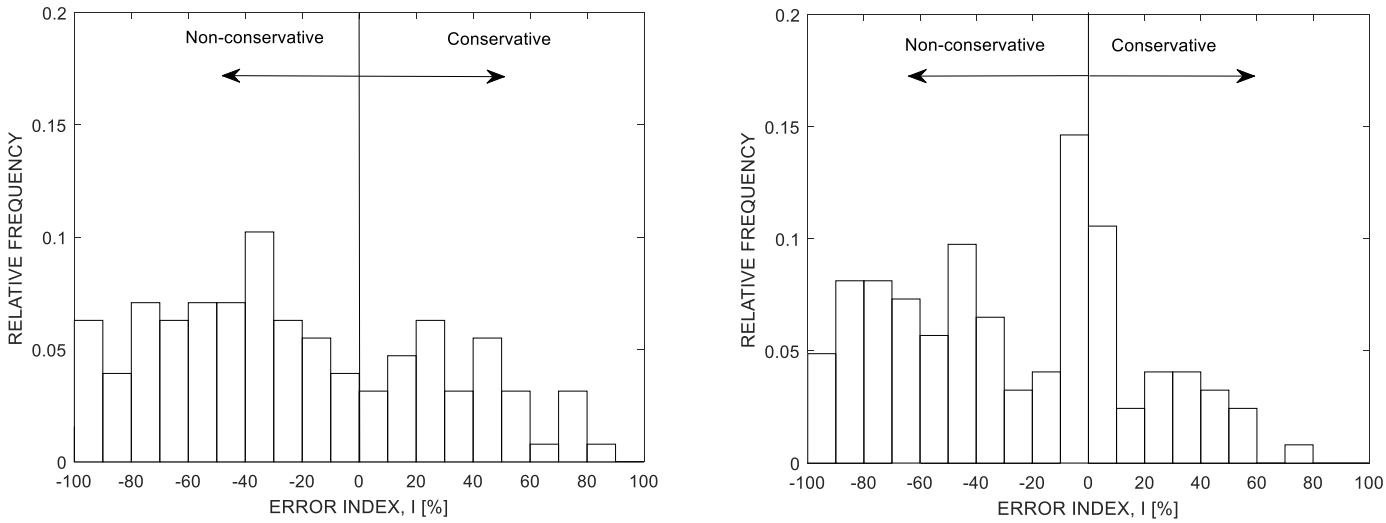

Fig.4. 26 Experimental cycles to failure and predicted cycles to failure with a) iteration method and b) constant coefficient method

As can be seen from the Figure above, both methods tends to give non-conservative estimation for the data examined.

5. Conclusion

In this thesis, fracture plane orientation determination method is proposed. The method is easy to apply and can give satisfied estimation of the fracture orientation for 48 experimental data examined related to hard steel, mild steal and cast iron.

58 experiment data related to fatigue limit loading condition is analyzed for smooth specimens subjected to proportional or non-proportional loading with different mean stress values and various stress ratios by various critical plane method. The proposed PDMR based critical plane methods show a good estimation capacity as compared to other critical plane methods from literature.

Fatigue life of 123 experimental data about circular tube-to-plate welded joints under tension, torsion, proportional or non-proportional combined tension and torsion loading analyzed by the proposed method based on nominal stresses. The proposed method shows a satisfied estimation capacity. But the estimation for non-proportional loading tends to be non-conservative.

Bibliography

Anderson, T. (2005). *Fracture Mechanics: Fundamentals and Application.* CRC Press.

Anes, V., Reis, L., Li, B., Fonte, M., & Freitas, M. d. (2014, May). New approach for analysis of complex multiaxial loading paths. *International journal of fatigue, 62*, 21-33.

Araújo, J., Dantas, A., Castro, F., Mamiya, E., & Ferreira, J. (2011, August). On the characterization of the critical plane with a simple and fast alternative measure of the shear stress amplitude in multiaxial fatigue. *International Journal of Fatigue, 33*(8), 1092–1100.

B. Li, L. R., & Freitas, M. d. (2009, November-December). Comparative study of multiaxial fatigue damage models for ductile structural steels and brittle materials. *International Journal of Fatigue, 31*(11-12), 1895-1906.

Bannantine, J. A., & Socie, D. F. (1992). A Multiaxial Fatigue Life Estimation Technique. In M. R. Mitchell, & R. W. Landgraf (Eds.), *Advances in Fatigue Lifetime Predictive Techniques* (pp. 249-275). Philadelphia: American Society for Testing and Materials.

Bruun, Ø. A. (2013). *Fatigue Assessment of Components Subjected to Non-Proportional Stress Histories.* Master Thesis.

Carpinteri, A., & Spagnoli, A. (2001). Multiaxial high-cycle fatigue criterion for hard metals. *International Journal of Fatigue, 23*(2), 135–145.

Carpinteri, A., & Spagnoli, A. (2001). Multiaxial high-cycle fatigue criterion for hard metals. *International Journal of Fatigue, 23*(2), 135–145.

Carpinteri, A., Brighenti, R., Macha, E., & Spagnoli, A. (1999, January). Expected principal stress directions under multiaxial random loading. Part II: numerical simulation and experimental assessment through the weight function method. *International Journal of Fatigue, 21*(1), 89–96.

Carpinteri, A., Ronchei, C., Spagnoli, A., & Vantadori, S. (2014, November). On the use of the Prismatic Hull method in a critical plane-based multiaxial fatigue criterion. *International Journal of Fatigue, 68*, 159–167.

Carpinteri, A., Spagnoli, A., & Vantadori, S. (2009, January). Multiaxial fatigue life estimation in welded joints using the critical plane approach. *International Journal of Fatigue, 31*(1), 188-916.

Carpinteri, A., Spagnoli, A., & Vantadori, S. (2011, August). Multiaxial fatigue assessment using a simplified critical plane-based criterion. *International Journal of Fatigue, 33*(8), 969-976.

Carpinteri, Brighenti, & Spagnoli. (2000, April). A fracture plane approach in multiaxial high-cycle fatigue of metals. *Fatigue & Fracture of Engineering Materials & Structures, 23*(4), 355-364.

Carpinteria, A., Machab, E., Brighentia, R., & Spagnoli, A. (1999, January). Expected principal stress directions under multiaxial random loading. Part I: theoretical aspects of the weight function method. *International Journal of Fatigue, 21*(1), 83-88.

Chen, X., Gao, Q., & Sun, X. (1994, April). Damage analysis of low-cycle fatigue under non-proportional loading. *International Journal of Fatigue, 16*(3), 221-5.

Crossland, B. (1956). Effect of large hydrostatic pressures on thetorsional fatigue strength of an alloy steel. *In: Proceedings of the international conference on fatigue of metals*, 138-49.

Dong, P., Wei, Z., & Hong, J. K. (2010, April). A path-dependent cycle counting method for variable-amplitude multi-axial loading. *International Journal of Fatigue, 32*(4), 720–734.

Dowling, N. E. (2009, December). Mean stress effects in strain-life fatigue. *Fatigue & Fracture of Engineering Materials & Structures, 32*(12), 1004–1019.

Findley, W. N. (1957). Fatigue of Metals Under Combinations of Stresses. *Transaction ASME*, 1337-48.

Gerber, W. (1874). Bestimmung der zulässigenSpannungen in Eisen-Konstruktionen(Calculation of the allowable stresses in iron structures). *ZBayer Archit Ing-Ver, 6*, 101-110.

Gonçalves, C. A., Araújo, J. A., & Mamiya, E. N. (2005, February). Multiaxial fatigue: a stress based criterion for hard metals. *International Journal of Fatigue, 27*(2), 177-187.

Goodman, J. (1899). *Mechanics applied to engineering.* Longmans: Green &Co.

Gough, H. J., & Pollard, H. V. (1935). The strength of metals under combined alternating stresses. *Proceedings of the institution of mechanical engineers, 1–103*.

K, D. V., G, C., JF, F., A, L. D., & HP, L. (1989). Criterion for high cycle fatigue failure under multiaxial loading. In M. W. Brown, & K. J. Miller (Eds.), *Biaxial and multiaxial fatigue* (pp. 459-478). London: Mechanical Engineering publications.

Karolczuk, A., & Kluger, K. (2014, October). Analysis of the coefficient of normal stress effect in chosen multiaxial fatigue criteria. *Theoretical and Applied Fracture Mechanics, 73*, 39-47.

Kluger, K. (2015, November). Fatigue life estimation for 2017A-T4 and 6082-T6 aluminium alloys subjected to bending-torsion with mean stress. *International Journal of Fatigue, 80*, 22–29.

Lee, S.-B. (1985). A criterion for fully reversed out-of-phase torsion and bending. (K. J. Miller, & M. W. Brown, Eds.) *Multiaxial Fatigue*, 553-568.

Lemaitre, J., & Chaboche, J.-L. (1990). *Mechanics of Solid Materials.* Cambridge: Cambridge University Press.

Li, B., Jiang, C., Han, X., & Li, Y. (2015, september). A new approach of fatigue life prediction for metallic materials under multiaxial loading. *International journal of fatigue, 78*, 1-10.

Li, B., Reis, L., & Freitas, M. d. (2009, November-December). Comparative study of multiaxial fatigue damage models for ductile structural steels and brittle materials. *International Journal of Fatigue, 31*(11-12), 1895-1906.

Mamiya, E. N., & Araújo, J. A. (2002, March-April). Fatigue limit under multiaxial loadings: on the definition of the equivalent shear stress. *Mechanics Research Communications, 29*(2-3), 141-151.

Mamiya, E., Araújo, J., & Castro, F. (2009, July). Prismatic hull: A new measure of shear stress amplitude in multiaxial high cycle fatigue. *International Journal of Fatigue, 31*(7), 1144-1153.

Mamiya, E., Castro, F., Algarte, R., & Araújo, J. (2011, April). Multiaxial fatigue life estimation based on a piecewise ruled S–N surface. *International Journal of Fatigue, 33*(4), 529–540.

Mamiya, E., Castro, F., Algarte, R., & Araújo, J. (2011, April). Multiaxial fatigue life estimation based on a piecewise ruled S–N surface. *International Journal of Fatigue, 33*(4), 529–540.

Matake, T. (1977, March). An Explanation on Fatigue Limit under Combined Stress. *Bulletin of JSME, 20*(141), 257-263.

McDiarmid, D. L. (1991, April). A general criterion for high cycle multiaxial fatigue failure. *Fatigue & Fracture of Engineering Materials & Structures, 14*(4), 429–453.

McDiarmid, D. L. (1994, December). A shear stress based critical-plane criterion of multiaxial fatigue failure for design and life prediction. *Fatigue & Fracture of Engineering Materials & Structures, 17*(12), 1475–1484.

Meggiolaro, M. A., & Castro, J. T. (2012, September). An improved multiaxial rainflow algorithm for non-proportional stress or strain histories – Part I: Enclosing surface methods. *International Journal of Fatigue, 42*, 217-226.

Niemi, E. (1995). *Stress Determination for Fatigue Analysis of Welded Components.* The international Institute of Welding.

Papadopoulos, I. (1998, March). Critical plane approaches in high-cycle fatigue: on the definition of the amplitude and mean value of the shear stress acting on the critical plane. *Fatigue & Fracture of Engineering Materials & Structures, 21*(3), 269–285.

Papadopoulos, I. V. (2001, November). Long life fatigue under multiaxial loading. *International Journal of Fatigue, 23*(10), 839–849.

Radaj, D., Sonsino, C., & Fricke, W. (2006). *Fatigue assessment of welded joints by local approaches.* Cambridge: Woodhead Publishing Limited.

Sines, G., Waisman, J., & Dolan, T. (1959). *Metal Fatigue.* New York: McGraw-Hill.

Socie, D. F., & Marquis, G. B. (2000). *Multiaxial Fatigue.* Warrendale: Society of Automotive Engineers Inc.

Sonsino, C. M., & Kueppers, M. (2001, May). Multiaxial fatigue of welded joints under constant and variable amplitude loadings. *Fatigue & Fracture of Engineering Materials & Structures, 24*(5), 309–327.

SUSMEL, L., & TOVO, R. (2004). On the use of nominal stresses to predict the fatigue strength of welded joints under biaxial cyclic loading. *Fatigue & Fracture of Engineering Materials & Structures, 27*(11), 1005–1024.

Susmela, L., Tovoa, R., & Lazzarin, P. (2005, August). The mean stress effect on the high-cycle fatigue strength from a multiaxial fatigue point of view. *International Journal of Fatigue, 27*(8), 928–943.

V, G., & A., S. (1976). Fatigue under combined out-of-phase multiaxial stresses. *In: Proceedings of international conference on fatigue testing and design*, 27.1-8.

Wang, C. H., & Brown, M. W. (1996, July). Life Prediction Techniques for Variable Amplitude Multiaxial Fatigue—Part 1: Theories. *Journal of Engineering Materials and Technology, 118*(3), 367-370.

Wang, Y., & Yao, W. (2004, January). Evaluation and comparison of several multiaxial fatigue criteria. *International Journal of Fatigue, 26*(1), 17-25.

Wei, Z., & Dong, P. (2010, October). Multiaxial fatigue life assessment of welded structures. *Engineering Fracture Mechanics, 77*(15), 3011–3021.

You, B.-R., & Lee, S.-B. (1996). A critical review on multiaxial fatigue assessments of metals. *International Journal of Fatigue, 18*(4), 235–244.

Zouain, N., Mamiya, E. N., & Comes, F. (2006, January-February). Using enclosing ellipsoids in multiaxial fatigue strength criteria. *European Journal of Mechanics - A/Solids, 25*(1), 51-71.

APPENDIX A Experimental data from (Carpinteri A. , Brighenti, Macha, & Spagnoli, 1999) and theoretical fracture plane orientation estimated by C-S and two proposed PDMR based methods

Material	No	α (°)	β (°)	$\sigma_{x,a}$ (MPa)	$\sigma_{x,m}$ (MPa)	$\sigma_{y,a}$ (MPa)	$\sigma_{y,m}$ (MPa)	$\tau_{xy,a}$ (MPa)	$\tau_{xy,m}$ (MPa)	η_{exp} (°)	CS (°)	Proposed 1 (°)	Proposed 2 (°)	Proposed 3 (°)
Hard steel	1	0	0	0.0	0.0	0.0	0.0	225.63	0.0	45	45	45	45	45
	2	0	0	0.0	0.0	0.0	0.0	201.11	0.0	45	45	45	45	45
	3	0	0	162.85	0.0	0.0	0.0	195.69	0.0	35	34	34	34	34
	4	0	0	141.85	0.0	0.0	0.0	171.28	0.0	34	34	34	34	34
	5	0	0	274.68	0.0	0.0	0.0	137.34	0.0	23	23	23	22	22
	6	0	0	255.06	0.0	0.0	0.0	127.53	0.0	22	23	23	22	22
	7	0	0	344.33	0.0	0.0	0.0	71.32	0.0	12	12	11	11	11
	8	0	0	308.03	0.0	0.0	0.0	63.86	0.0	12	12	11	11	11
	9	0	0	353.16	0.0	0.0	0.0	0.0	0.0	0	0	0	0	0
	10	0	0	323.73	0.0	0.0	0.0	0.0	0.0	0	0	0	0	0
	11	0	30	152.35	0.0	0.0	0.0	183.94	0.0	23	34	30	33	33
	12	0	30	141.95	0.0	0.0	0.0	171.18	0.0	32	34	30	33	33
	13	0	30	264.87	0.0	0.0	0.0	132.44	0.0	16	22	20	21	21
	14	0	30	255.06	0.0	0.0	0.0	127.53	0.0	16	22	19	21	21
	15	0	60	157.65	0.0	0.0	0.0	190.31	0.0	23	41	18	34	34
	16	0	60	147.15	0.0	0.0	0.0	177.56	0.0	22	39	18	34	34
	17	0	60	264.87	0.0	0.0	0.0	132.44	0.0	8	18	11	17	17
	18	0	60	255.06	0.0	0.0	0.0	127.53	0.0	8	18	11	17	17
	19	0	90	162.85	0.0	0.0	0.0	196.69	0.0	25	62	0	37	38
	20	0	90	152.45	0.0	0.0	0.0	184.23	0.0	29	62	0	37	38
	21	0	90	294.30	0.0	0.0	0.0	147.15	0.0	0	88	0	0	0
	22	0	90	264.87	0.0	0.0	0.0	132.44	0.0	0	88	0	0	0
	23	0	90	344.33	0.0	0.0	0.0	71.32	0.0	0	87	0	0	0
	24	0	90	308.03	0.0	0.0	0.0	63.86	0.0	0	87	0	0	0
Carbon steel	25	0	0	227.6	0.0	2.0	0.0	0.0	0.0	0	0	0	0	0
	26	0	0	233.5	52.0	191.3	41.2	0.0	0.0	0	0	0	0	0

	27	0	0	171.7	-24.5	228.6	-11.8	0.0	0.0	90	90	90	90	90
	28	0	0	121.6	11.8	156.0	-7.8	0.0	0.0	90	90	90	90	90
	29	180	0	6.9	0.0	224.6	-2.9	0.0	0.0	90	90	90	90	90
	30	180	0	155.0	79.0	118.7	0.0	0.0	0.0	0	0	0	0	0
Mild steel	31	0	0	245.3	0.0	0.0	0.0	0.0	0.0	0	0	0	0	0
	32	0	0	235.6	0.0	0.0	0.0	48.9	0.0	12	12	11	11	11
	33	0	0	187.3	0.0	0.0	0.0	93.6	0.0	22	23	23	22	22
	34	0	0	101.3	0.0	0.0	0.0	122.3	0.0	30	34	34	34	34
	35	0	0	0.0	0.0	0.0	0.0	142.3	0.0	45	45	45	45	45
	36	0	60	194.2	0.0	0.0	0.0	97.1	0.0	12	18	11	17	18
	37	0	60	108.9	0.0	0.0	0.0	131.5	0.0	8	35	18	34	34
	38	0	90	235.6	0.0	0.0	0.0	48.9	0.0	0	0	0	0	0
	39	0	90	208.1	0.0	0.0	0.0	104.1	0.0	8	8	0	0	0
	40	0	90	112.6	0.0	0.0	0.0	136.0	0.0	39	39	0	38	38
Cast iron	41	0	0	93.2	0.0	0.0	0.0	0.0	0.0	0	0	0	0	0
	42	0	0	95.2	0.0	0.0	0.0	19.7	0.0	12	12	11	11	11
	43	0	0	83.4	0.0	0.0	0.0	41.6	0.0	25	23	22	22	22
	44	0	0	56.3	0.0	0.0	0.0	68.0	0.0	34	34	34	34	34
	45	0	0	0.0	0.0	0.0	0.0	94.2	0.0	49	45	45	45	45
	46	0	90	104.2	0.0	0.0	0.0	21.6	0.0	0	0	0	0	0
	47	0	90	97.1	0.0	0.0	0.0	48.6	0.0	0	8	0	0	0
	48	0	90	71.3	0.0	0.0	0.0	86.1	0.0	37	39	0	0	38

APPENDIX B Fatigue properties of the experiment components (Carpinteri, Ronchei, Spagnoli, & Vantadori, 2014)

Authors	Material	σ_u/f_y (MPa)	σ_{af} (MPa)	τ_{af} (MPa)	$\frac{\tau_{af}}{\sigma_{af}}$
Nishihara et al.	Hard steel	681	313.9	196.2	0.63
	Mild steel	374	235.4	137.3	0.58
	Cast steel	181	96.1	91.2	0.95
Froustey et al.	30NCD16	1880	660	410.0	0.62
Bhongb hibhat	St35	340	230.0	130	0.57
	42CrMo4V	1003	485.0	315	0.65
Zenner et al.	25CrMo4	780	361.0	228.0	0.63
Troost et al.	25CrMo4	660	340	228.0	0.67
Heidenreich et al.	34Cr4	550	343	204	0.59
Kaniut	25CrMo4	780	361	228	0.67
McDiarmid	En24T	850	405	270	0.67
-	Stahl ausser diesen	1000	450	259.7	0.58

APPENDIX C Loading conditions of experimental tests collected in (Carpinteri, Ronchei, Spagnoli, & Vantadori, 2014)

Material	No	Path type	α(°)	β(°)	λ_{xy}, λ_y(-)	$\sigma_{x,a}(MPa)$	$\sigma_{x,m}(MPa)$	$\sigma_{y,a}(MPa)$	$\sigma_{y,m}(MPa)$	$\tau_{xy,a}(MPa)$	$\tau_{xy,m}(MPa)$	γ(°)
Hard steel	1	(a.1)	0	0	1	131.8	0.0	0.0	0.0	167.1	0.0	75
	2		0	0	1	245.3	0.0	0.0	0.0	122.7	0.0	64
	3		0	0	1	299.1	0.0	0.0	0.0	62.8	0.0	53
Mild steel	4	(a.1)	0	0	1	99.9	0.0	0.0	0.0	120.9	0.0	78
	5		0	0	1	180.3	0.0	0.0	0.0	90.2	0.0	67
	6		0	0	1	213.2	0.0	0.0	0.0	44.8	0.0	56
Cast iron	7	(a.1)	0	0	1	56.3	0.0	0.0	0.0	68.0	0.0	46
	8		0	0	1	83.4	0.0	0.0	0.0	41.6	0.0	29
	9		0	0	1	95.2	0.0	0.0	0.0	19.7	0.0	18
30NCD16	10	(a.1)	0	0	1	485.0	0.0	0.0	0.0	280.0	0.0	66
St35	11	(a.2)	0	0	1	160.0	176.0	160.0	176.0	0.0	0.0	61
42CrMo4V	12	(a.2)	0	0	1	402.0	442.0	201.0	221.0	0.0	0.0	39
Hard steel	13	(b.1)	0	30	1	140.4	0.0	0.0	0.0	169.9	0.0	75
	14		0	30	1	249.7	0.0	0.0	0.0	124.9	0.0	63
	15		0	60	1	145.7	0.0	0.0	0.0	176.3	0.0	77
	16		0	60	1	252.4	0.0	0.0	0.0	126.2	0.0	59
	17		0	90	1	150.2	0.0	0.0	0.0	181.7	0.0	80
	18		0	90	1	258.0	0.0	0.0	0.0	129.0	0.0	41
	19		0	90	1	304.5	0.0	0.0	0.0	63.9	0.0	41
Mild steel	20	(b.1)	0	60	1	103.6	0.0	0.0	0.0	125.4	0.0	80
	21		0	60	1	191.4	0.0	0.0	0.0	95.7	0.0	62
	22		0	90	1	108.9	0.0	0.0	0.0	131.8	0.0	84
	23		0	90	1	201.1	0.0	0.0	0.0	100.6	0.0	45
	24		0	90	1	230.2	0.0	0.0	0.0	48.3	0.0	45
Cast iron	25	(b.1)	0	60	1	67.6	0.0	0.0	0.0	81.6	0.0	42
	26		0	60	1	93.7	0.0	0.0	0.0	46.9	0.0	25
	27		0	90	1	73.2	0.0	0.0	0.0	88.4	0.0	46
	28		0	90	1	101.9	0.0	0.0	0.0	21.1	0.0	7

St35	29	(b.1)	90	0	1	140.0	154.0	140.0	154.0	0.0	0.0	46
	30		180	0	1	120.0	132.0	120.0	132.0	0.0	0.0	46
42CrMo4V	31	(b.1)	90	0	1	402.0	442.0	201.0	221.0	0.0	0.0	39
30NCD16	32	(b.1)	0	0	1	211.0	300.0	0.0	0.0	365.0	0.0	69
	33		0	0	1	480.0	300.0	0.0	0.0	277.0	0.0	59
	34		0	0	1	590.0	300.0	0.0	0.0	148.0	0.0	51
	35		0	45	1	480.0	300.0	0.0	0.0	277.0	0.0	57
	36		0	45	1	565.0	300.0	0.0	0.0	141.0	0.0	48
	37		0	60	1	470.0	300.0	0.0	0.0	270.0	0.0	54
	38		0	90	1	473.0	300.0	0.0	0.0	273.0	0.0	41
	39		0	90	1	480.0	0.0	0.0	0.0	277.0	0.0	41
	40		0	90	1	540.0	300.0	0.0	0.0	135.0	0.0	41
25CrMo4	41	(b.2)	0	60	1	155.0	340.0	0.0	170.0	155.0	0.0	44
	42		0	60	1	220.0	340.0	0.0	170.0	110.0	0.0	42
	43		0	90	1	159.0	340.0	0.0	170.0	159.0	0.0	41
	44		0	90	1	233.0	340.0	0.0	170.0	117.0	0.0	41
25CrMo4	45	(b.2)	0	90	1	208.0	255.0	156.0	210.0	104.0	0.0	39
	46		60	90	1	225.0	255.0	169.0	210.0	113.0	0.0	37
	47		90	45	1	222.0	255.0	167.0	210.0	111.0	0.0	42
	48		90	90	1	205.0	255.0	154.0	210.0	103.0	0.0	37
	49		90	135	1	215.0	255.0	161.0	210.0	108.0	0.0	40
	50		180	90	1	224.0	255.0	168.0	210.0	112.0	0.0	37
34Cr4	51	(c)	0	0	2	200.0	244.0	200.0	244.0	0.0	0.0	44
25CrMo4	52	(c)	0	0	1/4	210.0	0.0	0.0	0.0	105.0	0.0	48
	53		0	90	2	220.0	0.0	0.0	0.0	110.0	0.0	60
	54		0	0	2	242.0	0.0	0.0	0.0	121.0	0.0	58
	55		0	0	8	196.0	0.0	0.0	0.0	98.0	0.0	60
En24T	56	(c)	180	0	3	260.0	0.0	260.0	0.0	0.0	0.0	55
St35	57	(c)	0	0	2	130.0	143.0	130.0	143.0	0.0	0.0	90
	58		90	0	2	140.0	154.0	140.0	154.0	0.0	0.0	46

APPENDIX D Critical plane orientation, γ, and error index, I.

Test No.	Critical plane orientation (°)			Findley	McDiarmid	Matake	Dang Van	Papadopoulos	Carpinteri -Spagnoli	PDMR First/Second	PDMR SWT
	γ_{cs}	γ_{PDMR}	γ_{PDMR_SWT}	$I_{PH}(\%)$	$I_{PH}(\%)$	$I_{PH}(\%)$	$I_{PH}(\%)$	$I_{PH}(\%)$	$I_{PH}(\%)$	$I_{PDMR}(\%)$	$I_{PDMR}(\%)$
1	75	75	75	3.23	-3.60	-0.03	-0.05	-2.21	-4.85	-4.88	-4.88
2	64	63	63	7.50	-2.60	4.00	4.10	4.82	-0.81	-0.71	-0.71
3	53	52	52	5.07	-6.34	1.74	1.73	6.00	-1.55	-1.49	-1.49
4	78	78	78	2.77	2.00	1.36	1.33	-0.88	-2.22	-2.24	-2.24
5	67	67	67	5.30	4.90	3.78	3.82	4.62	0.78	0.91	0.91
6	56	56	56	-1.50	-1.55	-2.87	-2.88	1.42	-4.02	-3.93	-3.93
7	40	41	41	146.36	-11.50	8.48	8.38	6.51	5.46	5.44	5.44
8	29	29	29	140.10	-23.90	5.56	5.61	6.18	4.08	4.11	4.11
9	18	18	18	134.90	-30.30	3.48	3.32	6.24	2.50	2.50	2.50
10	66	66	66	7.87	-3.27	4.57	4.65	4.71	-0.29	-0.17	-0.17
11	90	46	49	-29.89	-26.67	-30.40	-4.72	-30.90	-15.00	21.33	0.81
12	39	39	39	-13.20	-26.10	-17.10	23.9	7.10	-1.18	6.22	0.99
13	75	74	74	5.80	-3.20	0.23	1.10	0.16	-4.40	-4.26	-4.26
14	63	62	62	8.10	-2.58	5.16	2.80	6.04	-1.86	-1.04	-1.04
15	76	75	75	9.40	-4.90	-2.60	1.25	3.38	-6.41	-6.46	-6.46
16	58	58	58	5.10	-6.89	1.73	-2.52	5.62	-8.48	-6.43	-6.43
17	80	78	78	12.30	3.60	11.70	2.10	6.20	-9.74	-10.72	-10.72
18	42	41	41	6.10	-60	2.70	-1.40	6.90	-10.00	-2.99	-2.99
19	41	41	41	4.60	-7.40	1.20	0.40	6.60	-3.36	-0.54	-0.54
20	80	79	79	4.90	-2.50	-2.90	-0.20	1.90	-5.15	-5.11	-5.11
21	62	62	62	4.40	4.40	2.90	-0.20	8.60	-4.10	-2.77	-2.77
22	84	83	83	9.40	10.50	9.20	2.60	6.80	-5.21	-5.43	-5.43
23	45	45	45	8.30	8.30	6.70	3.70	13.00	-5.06	1.67	1.67
24	45	45	45	3.50	3.50	2.00	1.50	8.20	-0.59	1.97	1.97
25	42	31	31	178.70	-3.00	10.90	24.90	27.00	14.13	23.29	23.29
26	24	19	19	165.80	-18.60	23.30	11.20	17.70	10.53	18.34	18.34
27	46	7	7	172.10	17.10	68.90	32.90	37.20	7.00	35.73	35.73

28	7	7	7	151.30	-27.10	10.40	8.40	12.80	7.81	11.44	11.44
29	46	44	44	-13.90	-9.30	-13.90	1.50	-16.80	-25.62	29.35	13.90
30	46	54	44	-6.90	-7.60	-7.70	5.50	-10.20	-36.25	0.60	-7.33
31	39	39	39	-4.80	-17.50	-7.50	24.10	9.60	-1.18	16.03	14.46
32	69	77	78	1.90	-4.50	-1.10	7.70	-0.10	-6.14	-4.89	-4.95
33	57	65	66	6.70	-4.30	3.50	12.40	6.80	3.03	0.30	0.47
34	51	55	55	0.90	-11.70	-2.00	6.80	4.70	0.82	-2.32	-1.29
35	57	62	63	4.00	-8.60	2.00	5.80	5.60	-3.32	-4.49	-4.42
36	48	51	51	-5.60	-18.20	-8.40	-0.70	-0.60	-5.40	-6.60	-5.33
37	54	60	61	-0.60	-13.90	-3.60	0.40	2.50	-9.44	-10.00	-10.13
38	42	42	42	-1.50	-14.70	-4.30	-0.28	2.40	-12.18	-4.87	-2.76
39	42	42	42	-0.10	-13.40	-2.90	-7.80	0.70	-17.57	-10.51	-10.50
40	42	42	42	-10.40	-22.50	-13.20	-5.20	-5.30	-11.86	-8.56	-6.80
41	44	59	71	-12.90	-20.90	-14.00	8.90	-5.40	-20.08	-8.61	-17.42
42	42	48	57	-20.10	-30.00	-22.90	3.20	-8.00	-14.17	-1.27	-13.19
43	41	41	73	-11.30	-20.10	-12.00	8.30	-3.60	-19.08	-1.66	-24.57
44	41	41	41	-16.20	-26.70	-19.30	6.80	-4.00	-10.79	4.14	-0.67
45	38	70	80	-18.70	-33.20	-23.60	19.00	3.70	-15.35	-3.39	-12.12
46	37	87	83	-1.50	-19.00	-7.40	29.50	17.50	-8.95	-1.30	-9.58
47	43	68	65	2.20	-16.00	-4.00	27.20	18.10	-0.91	22.36	14.81
48	37	46	81	-3.30	-20.40	-9.00	21.80	11.80	-15.47	20.76	-20.72
49	40	54	58	-1.00	-13.60	-2.80	30.30	14.10	-13.71	2.12	-13.07
50	37	37	41	5.30	-5.30	3.20	24.90	12.30	-9.57	23.6	13.06
51	44	73/47	47	2.90	2.20	2.60	25.20	6.80	-27.26	1.04/71.24	-17.73
52	59	38/37	37	-3.50	-13.50	-6.50	-10.20	-6.70	-26.20	-31.35/-12.00	-12.00
53	18	38/37	37	47.30	52.40	46.00	43.20	50.50	-30.00	-24.36/-23.06	-23.06
54	18	38/37	37	62.00	67.50	60.50	57.50	65.50	-0.40	7.40/21.40	21.40
55	60	37/37	37	45.60	50.20	44.20	41.30	47.90	-30.01	-31.43/10.20	10.20
56	38	82/37	53	8.00	-11.00	2.20	9.00	9.70	-38.40	-35.24/-6.02	-6.02
57	46	66/66	66	-0.50	4.80	-0.60	13.80	-3.20	-30.93	-2.61/20.72	-16.32
58	46	90/84	84	-4.80	0.00	-5.00	13.60	-8.20	-25.62	6.15/11.00	-30.76
average	-	-	-	27.1	14.2	10.4	10.9	10.6	10.6	8.9/9.6	8.7

APPENDIX E Fatigue properties (SUSMEL & TOVO, 2004)

Reference	Material	σ_u (MPa)	σ_{af} (MPa)	m	τ_{af} (MPa)	m^*	τ_{af}/σ_{af}
Yung et al.	A519	700	65.3	5.4	47.0	3.7	0.72
Siljander et al.	A519	700	89.2	3.8	74.8	5.5	0.84
Amstutz et al.	StE 460	670	84.2	5.4	75.5	6.2	0.90
Sonsino et al.	StE 460	670	109.4	4.4	88.2	4.8	0.81

APPENDIX F Loading conditions and fatigue life (SUSMEL & TOVO, 2004)

Reference	No	Path type	β(°)	$\sigma_{x,a}$ (MPa)	$\sigma_{x,m}$ (MPa)	$\tau_{xy,a}$ (MPa)	$\tau_{xy,m}$ (MPa)	N_{exp} (cycles)	N_{cal} (cycles)	N_{cal2} (cycles)
Yung et al.	1	A	0	115.0	0.0	0.0	0.0	76,660	198,320	35,000
	2		0	109.0	0.0	0.0	0.0	198,000	253,340	178,190
	3		0	100.5	0.0	0.0	0.0	145,690	366,570	273,190
	4		0	86.5	0.0	0.0	0.0	560,850	721,920	601,670
	5		0	79.5	0.0	0.0	0.0	624,330	1,054,000	938,100
	6	C	0	0.0	0.0	70	0.0	466,860	517,710	312,590
	7		0	0.0	0.0	60	0.0	827,560	935,700	703,590
	8	E	0	115	0.0	39.5	0.0	27,100	119,030	69,684
	9		0	109	0.0	62.5	0.0	47,090	79,147	39,573
	10		0	109	0.0	41.5	0.0	78,620	138,070	81,602
	11		0	86.5	0.0	50.0	0.0	93,690	218,510	132,060
	12		0	79.5	0.0	46.0	0.0	220,030	314,550	205,390
	13		0	65.0	0.0	37.5	0.0	788,370	745,450	592,280
Siljander et al.	14	A	0	220.0	0.0	0.0	0.0	76,800	57,676	72,241
	15		0	158.5	0.0	0.0	0.0	276,400	224,590	254,950
	16		0	140.0	0.0	0.0	0.0	395,900	374,090	410,930
	17		0	110.0	0.0	0.0	0.0	729,900	1,002,000	1,038,900
	18	B	0	222.0	222.0	0.0	0.0	55,700	17,834	48,745
	19		0	140.0	140.0	0.0	0.0	270,390	183,750	277,270
	20		0	103.85	103.85	0.0	0.0	1,036,000	754,510	874,660
	21		0	110	110	0.0	0.0	1,300,140	578,160	701,030
	22	C	0	0.0	0.0	110.0	0.0	132,000	530,680	657,140
	23		0	0.0	0.0	85.0	0.0	1,605,000	1,732,800	1,771,400
	24		0	0.0	0.0	70.0	0.0	3,303,000	4,168,500	3,738,000
	25		0	0.0	0.0	70.0	0.0	1,989,000	4,168,500	3,738,000
	26	D	0	0.0	0.0	110.0	110.0	374,000	353,730	513,940
	27		0	0.0	0.0	85.0	85.0	919,600	1,261,900	1,385,400
	28	F	0	130.15	130.15	54.45	54.45	260,200	125,690	208,730
	29		0	130.15	130.15	54.45	54.45	274,700	125,690	208,730

	30		0	108.05	108.05	14.7	14.7	577,000	575,120	698,550
	31		0	108.05	108.05	14.7	14.7	748,600	575,120	698,550
	32		0	68.0	68.0	68.0	68.0	852,900	1,083,900	1,282,400
	33		0	87.0	87.0	36.3	36.3	1,196,100	865,440	985,780
	34		0	87.0	87.0	36.3	36.3	1,201,400	865,440	985,780
	35		0	87.0	87.0	36.3	36.3	1,699,800	865,440	985,780
	36	G	0	170.0	0.0	85.0	85.0	981,200	1,073,300	1,236,000
	37	J	-	87.0	87.0	36.3	36.3	111,500	630,680	488,330
	38		-	87.0	87.0	36.3	36.3	142,600	630,680	488,330
	39		-	87.0	87.0	36.3	36.3	167,900	630,680	488,330
	40		-	87.0	87.0	36.3	36.3	206,300	630,680	488,330
	41	K	-	87.0	87.0	36.3	36.3	352,500	407,490	556,260
	42		-	87.0	87.0	36.3	36.3	354,200	407,490	556,260
	43		-	87.0	87.0	36.3	36.3	644,500	407,490	556,260
Amstutz et al.	44	A	0	220.0	0.0	0.0	0.0	43,700	13,434	14,275
	45		0	150.0	0.0	0.0	0.0	129,400	103,590	107,160
	46		0	120.0	0.0	0.0	0.0	548,400	340,060	346,790
	47		0	120.0	0.0	0.0	0.0	865,000	340,060	346,790
	48		0	120.0	0.0	0.0	0.0	1,991,200	340,060	346,790
	49		0	120.0	0.0	0.0	0.0	142,500	340,060	346,790
	50	B	0	310.0	310.0	0.0	0.0	2,230	114	1,307
	51		0	260.0	260.0	0.0	0.0	2,925	531	3,300
	52		0	155.0	155.0	0.0	0.0	8,900	24,531	50,195
	53		0	130.0	130.0	0.0	0.0	63,750	78,457	126,680
	54		0	100.0	100.0	0.0	0.0	141,000	410,610	503,970
	55		0	90.0	90.0	0.0	0.0	2,324,000	781,800	877,470
	56	C	0	0.0	0.0	150.0	0.0	26,650	74,438	84,751
	57		0	0.0	0.0	150.0	0.0	51,520	74,438	84,751
	58		0	0.0	0.0	120.0	0.0	103,500	253,400	274,280
	59	D	0	0.0	0.0	155.0	155.0	36,000	20,603	43,630
	60		0	0.0	0.0	155.0	155.0	18,100	20,603	43,630
	61		0	0.0	0.0	135.0	135.0	43,680	51,399	90,275
	62		0	0.0	0.0	120.0	120.0	157,000	109,850	167,800

	63	E	0	100.0	0.0	100.0	0.0	72,400	63,350	68,162
	64		0	100.0	0.0	100.0	0.0	97,200	63,350	68,162
	65		0	85.0	0.0	85.0	0.0	253,750	152,000	160,330
	66	F	0	175.0	175.0	175.0	175.0	2,440	260	2,060
	67		0	125.0	125.0	125.0	125.0	15,100	3,698	12,100
	68		0	100.0	100.0	100.0	100.0	29,900	17,846	39,162
	69		0	80.0	80.0	80.0	80.0	49,940	78,354	126,740
	70		0	70.0	70.0	70.0	70.0	65,150	183,630	255,940
	71		0	90.0	90.0	90.0	90.0	183,700	36,241	68,186
	72	H	90	100.0	0.0	100.0	0.0	22,270	257,960	201,150
	73		90	110.0	0.0	110.0	0.0	24,040	15,313	12,180
	74		90	110.0	0.0	110.0	0.0	30,780	15,313	12,180
	75	I	90	155.0	155.0	155.0	155.0	7,470	3,411	10,842
	76		90	130.0	130.0	130.0	130.0	12,130	12,893	27,363
	77		90	105.0	105.0	105.0	105.0	34,160	58,237	84,206
	78		90	95.0	95.0	95.0	95.0	82,680	114,510	142,600
	79		90	82.0	82.0	82.0	82.0	279,030	300,980	309,370
	80		90	60.0	60.0	60.0	60.0	315,540	2,150,400	1,601,400
	81		90	73.0	73.0	73.0	73.0	631,740	633,220	570,450
Sonsino et al.	82	A	0	285.0	0.0	0.0	0.0	23,600	35,044	38,217
	83		0	280.0	0.0	0.0	0.0	26,850	37,915	41,274
	84		0	290.0	0.0	0.0	0.0	29,460	32,435	35,433
	85		0	280.0	0.0	0.0	0.0	31,870	37,915	41,274
	86		0	220.0	0.0	0.0	0.0	76,790	110,810	117,770
	87		0	190.0	0.0	0.0	0.0	159,200	212,610	222,780
	88		0	160.0	0.0	0.0	0.0	276,080	456,180	470,290
	89		0	185.0	0.0	0.0	0.0	367,200	239,350	250,160
	90		0	140.0	0.0	0.0	0.0	394,750	825,380	840,430
	91		0	150.0	0.0	0.0	0.0	588,800	607,590	622,620
	92		0	110.0	0.0	0.0	0.0	730,230	2,407,100	2,398,100
	93		0	120.0	0.0	0.0	0.0	3,319,300	1,636,100	1,642,800
	94	C	0	0.0	0.0	230.0	0.0	16,400	36,267	45,606
	95		0	0.0	0.0	220.0	0.0	19,855	44,533	55,330

	96		0	0.0	0.0	217.0	0.0	21,480	47,448	58,734
	97		0	0.0	0.0	180.0	0.0	65,280	112,460	132,400
	98		0	0.0	0.0	110.0	0.0	373,080	1,089,100	1,126,600
	99		0	0.0	0.0	140.0	0.0	469,260	358,450	394,840
	100		0	0.0	0.0	120.0	0.0	826,200	729,420	771,770
	101		0	0.0	0.0	105.0	0.0	821,100	1,349,300	1,379,200
	102		0	0.0	0.0	85.0	0.0	918,700	3,569,000	3,456,400
	103		0	0.0	0.0	104.0	0.0	1,483,600	1,410,100	1,437,800
	104		0	0.0	0.0	90.0	0.0	1,503,800	2,743,500	2,695,900
	105		0	0.0	0.0	105.0	0.0	2,007,250	1,349,300	1,379,200
	106		0	0.0	0.0	80.0	0.0	3,398,530	4,717,100	4,498,900
	107		0	0.0	0.0	80.0	0.0	3,629,400	4,717,100	4,498,900
	108	E	0	172.0	0.0	100.0	0.0	54,600	102,500	111,800
	109		0	172.0	0.0	100.0	0.0	72,260	102,500	111,800
	110		0	165.0	0.0	96.0	0.0	86,400	123,490	133,940
	111		0	160.0	0.0	93.0	0.0	119,960	141,750	153,110
	112		0	123.0	0.0	72.5	0.0	320,780	460,590	480,390
	113		0	123.0	0.0	72.5	0.0	357,130	460,590	480,390
	114		0	125.0	0.0	72.5	0.0	858,360	428,490	447,860
	115	H	90	162.0	0.0	94.0	0.0	24,260	182,210	130,570
	116		90	165.0	0.0	95.7	0.0	25,900	167,810	120,560
	117		90	168.0	0.0	97.4	0.0	29,350	154,770	111,470
	118		90	125.0	0.0	72.5	0.0	51,970	582,870	403,120
	119		90	125.0	0.0	72.5	0.0	79,640	582,870	403,120
	120		90	126.0	0.0	73.1	0.0	99,560	562,420	389,390
	121		90	122.0	0.0	71.0	0.0	346,670	649,920	448,030
	122		90	80.0	0.0	46.4	0.0	728,060	4,302,300	2,806,300
	123		90	80.0	0.0	46.4	0.0	2,267,300	4,302,300	2,806,300